

Optimizing Multi-Modal Trackers via Sensitivity-aware Regularized Tuning

Zhiwen Chen, Jinjian Wu, *Senior Member, IEEE*, Zhiyu Zhu, Yifan Zhang, Guangming Shi, *Fellow, IEEE*, Junhui Hou, *Senior Member, IEEE*

Abstract—This paper tackles the critical challenge of optimizing multi-modal trackers by effectively adapting the pre-trained models for RGB data. Existing fine-tuning paradigms oscillate between excessive freedom and over-restriction, both leading to a suboptimal plasticity-stability trade-off. To mitigate this dilemma, we propose a novel sensitivity-aware regularized tuning framework, which delicately refines the learning process by incorporating intrinsic parameter sensitivities. Through a comprehensive investigation from pre-trained to multi-modal contexts, we identify that parameters sensitive to pivotal foundational patterns and cross-domain shifts are primary drivers of this issue. Specifically, we first analyze the tangent space of pre-trained weights to measure and orient prior sensitivities, dedicated to preserving generalization. Then, we further explore transfer sensitivities during the tuning phase, emphasizing adaptability and stability. By incorporating these sensitivities as regularization terms, our method significantly enhances the transferability across modalities. Extensive experiments showcase the superior performance of the proposed method, surpassing current state-of-the-art techniques across various multi-modal tracking. The source code and models will be publicly available at <https://github.com/zhiwen-xdu/SRTrack>.

Index Terms—Multi-modal Tracking, Cross-modal Transfer, Parameter Sensitivity, Regularized Tuning.

I. INTRODUCTION

OBJECT tracking, a foundation task of visual perception, has seen significant advancements over the past decades [1]–[4]. Despite the promising results, RGB-based trackers often struggle with some complex and degraded conditions, such as extreme illumination, motion blur, and occlusions. Therefore, multi-modal tracking with more comprehensive information (e.g., event, depth, thermal) has garnered growing interest. With the popularity of the data-driven methods in the object tracking community, both data scale and model

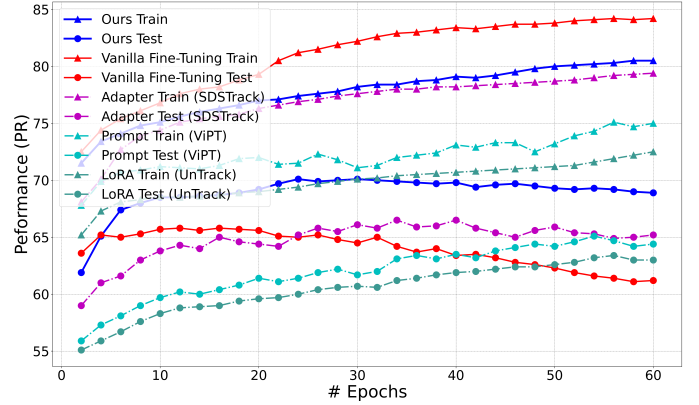


Fig. 1. Training and testing performance on LasHeR, comparing our method with existing fine-tuning approaches. Our method effectively mitigates the misfitting issue and enhances both generalization and stability of the multi-modal tracker.

size have experienced huge explosions [5]–[8]. There is a prevailing paradigm that explores pre-trained trackers on large-scale RGB-based datasets and adapts them to diverse auxiliary modalities, a process known as cross-modal fine-tuning or transfer learning, to enhance performance and accelerate convergence.

Some existing approaches have explored the *full fine-tuning* (FFT) paradigm [9]–[11], where these trackers are initialized with pre-trained weights and subsequently tuned for task-specific objectives. Nevertheless, due to the significant gap and limited scale of auxiliary modalities, they are intractable to retain the pre-trained knowledge during transfer and tend to induce catastrophic forgetting and **overfitting** (i.e., **widened train-test gap**). In contrast to full fine-tuning, recent research has shifted toward *parameter efficient fine-tuning* (PEFT) [12]–[14]. The PEFT keeps the majority of pre-trained parameters frozen, updating only a small fraction of modal-specific ones to retain pre-trained knowledge. Several methods fall under this umbrella [15]–[17], including prompt tuning, visual adapter, etc. While effective, PEFT methods impose excessive constraints on the primary model weights, resulting in **underfitting** (i.e., **restricted train upper bound**) for handling the vast distribution drift. In summary, existing tuning paradigms fluctuate between excessive flexibility and overly rigid constraints, both contributing to **misfitting** and a sub-optimal plasticity-stability trade-off between pre-trained knowledge and adaptation (please refer to Fig. 1).

In this work, we endeavor to mitigate the misfitting issue in cross-modal tracker adaptation by strategically regularizing the

This work was supported in part by the NSFC Excellent Young Scientists Fund 62422118, in part by the Hong Kong RGC under Grants 11219324 and 11219422, and in part by the Hong Kong ITC under Grant ITS/164/23. (Corresponding author: Jinjian Wu and Zhiyu Zhu)

Zhiwen Chen is with the School of Artificial Intelligence, Xidian University, Xi'an, China, and also with the Department of Computer Science, City University of Hong Kong (e-mail: zhiwen.chen@stu.xidian.edu.cn, zhiwen.chen@cityu.edu.hk).

Jinjian Wu and Guangming Shi are with the School of Artificial Intelligence, Xidian University, China. (e-mail: jinjian.wu@mail.xidian.edu.cn; gmshi@xidian.edu.cn).

Zhiyu Zhu and Junhui Hou are with the Department of Computer Science, City University of Hong Kong. (e-mail: zhiyuzhu2-c@my.cityu.edu.hk; jh.hou@cityu.edu.hk).

Yifan Zhang is with the School of Mechatronic Engineering and Automation, Shanghai University, Shanghai, China, and also with the Department of Computer Science, City University of Hong Kong. (e-mail: yfzhang@shu.edu.cn).

learning process. By examining parameter responses spanning from the pre-training to fine-tuning phases, we identify that pronounced parameter sensitivities are the primary cause of degraded prior generalizability and transfer adaptability. To mitigate this, we propose a sensitivity-aware regularized tuning framework that delicately calibrates the gradient updates to boost model transfer with precision. Specifically, we optimize multi-modal trackers from the following perspectives.

- (1) **Formulating Prior Sensitivity.** We begin by investigating the tangent space of pre-trained parameters, using it as a critical indicator to assess and preserve prior generalizability. Moreover, we estimate such prior sensitivity via an eigen-decomposition approximation.
- (2) **Modeling Transfer Sensitivity.** To further elucidate transfer challenges, we explore how sparse gradients exacerbate tuning instability. Accordingly, we construct this transfer sensitivity using the off-the-shelf gradient matrix, with the aim of facilitating gradient rebalancing.
- (3) **Sensitivity-Aware Regularization Tuning.** By harnessing the identified parameter sensitivities, we suggest an adaptive tuning scheme that safeguards essential pre-trained knowledge and fosters coherent multi-modal representations through finely modulated, sensitivity-driven updates. This regularization tuning facilitates seamless transfer to various multi-modal tracking tasks, which can continuously enhance the model in the training phase.

Our method strategically guides the cross-modal fine-tuning process to optimize downstream tracking tasks. Extensive experimental results showcase our method achieves new state-of-the-art results across three multi-modal tracking tasks (RGB-Event, RGB-Depth, RGB-Thermal) and seven benchmarks, spanning diverse pre-trained tracking models. Comprehensive ablation studies demonstrate the effectiveness of the sensitivity-aware regularization fine-tuning concept.

In summary, the main contributions of this paper are:

- we revisit the misfitting issue of multi-modal tracking for adapting foundation models and propose a novel regularized tuning framework to indicate better transferability, which is orthogonal to the existing FFT and PEFT methods;
- we formulate the parameter sensitivity with respect to pre-trained knowledge and transfer stability, and introduce a sensitivity-aware update strategy to refine the learning process, thereby facilitating the generalization and adaptability of multi-modal trackers;
- we conduct comprehensive experiments covering three multi-modal tracking tasks and seven datasets using diverse pre-trained trackers, and consistently push cross-modal tracking accuracy to new levels;

The remainder of the paper is organized as follows. Section II reviews existing works on multi-modal trackers and cross-modal transfer learning methods. In Section III, we explicitly formulate the prior and transfer sensitivity from both the pre-training and fine-tuning perspectives, followed by the implementation of sensitivity-aware regularized tuning. In Section IV, we present experiments on seven multi-modal tracking benchmarks to demonstrate the effectiveness of our

method, along with comprehensive ablation studies to analyze the impact of different components and designs. Finally, Section V concludes the paper.

II. RELATED WORK

A. Multi-Modal Tracking

Object tracking, a cornerstone task in computer vision, involves predicting the position and scale of an object in future frames based on its initial appearance [18]–[21]. In recent years, due to the unreliability of RGB data in challenging scenarios, increasing studies are expected to integrate auxiliary modalities (e.g., event, depth, thermal data) to enhance tracking performance. These complementary signals compensate for the inherent limitations of RGB imagery [22]. For instance, event cameras provide robust dynamic scene information under extreme motion or lighting. Leveraging this, [23]–[28] combine RGB and event streams to predict objects in high-speed and low-dynamic scenarios. Meanwhile, depth data offers spatial cues that are particularly useful for handling occlusion and background clutter. [29]–[32] exploit this by incorporating depth maps into a tracking framework to improve robustness in crowded scenes. Similarly, thermal infrared imaging captures heat signatures independent of visible light, proves effective in low-illumination. [33]–[36] demonstrate that fusing thermal and RGB data can yield more reliable appearance representations.

In summary, these methods emphasize effective multi-modal interaction and fusion [9], [37]–[39]. With the emergence of large-scale RGB datasets and universal backbones (e.g., vision transformer), pre-trained trackers [5], [8], [40] have achieved remarkable generalization across diverse scenarios. These advances have shifted the paradigm toward transferring knowledge from pre-trained models in designing high-performance trackers. Multi-modal tracking is increasingly driven by reusing RGB pre-trained semantic priors, particularly when annotated multi-modal data are scarce or noisy. In this work, we target this challenge by focusing on optimizing the adaptation of pre-trained trackers for efficient cross-modal transfer.

B. Cross-modal Transfer Learning

To adapt pre-trained models for multi-modal tracking, two main transfer learning strategies have recently emerged. Some works follow the full fine-tuning (FFT) paradigm [9]–[11], [37], where the pre-trained models serve as initializations and are entirely re-trained on the target tasks. These methods require a shared or compact cross-modal feature space to inherit the generalization capability of the original model. Representatively, SUTrack [8] employs a single vision transformer with unified input representations for multiple modalities, avoiding task-specific customization. While often effective, one primary drawback may be innate to this paradigm: the contradiction between the paucity of large-scale downstream datasets and the huge appetites of cross-domain adaptation often leads to significant catastrophic forgetting or overfitting. To alleviate this, profiting from the affluent experience of

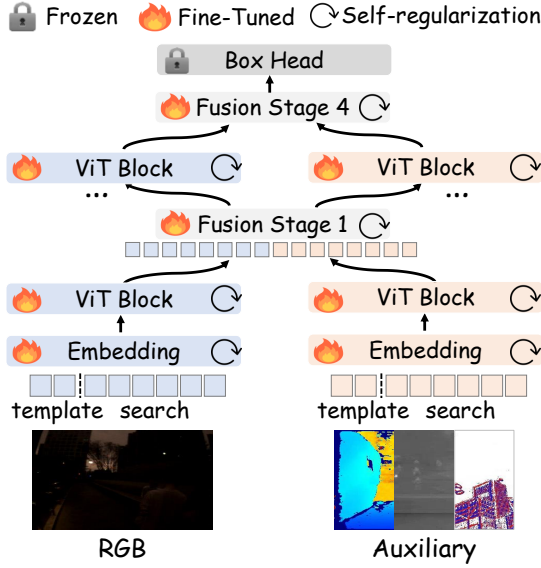


Fig. 2. Model architecture for our multi-modality tracker.

natural language processing and computer vision communities [12]–[14], some parameter-efficient fine-tuning (PEFT) methods have been proposed. The core principle of PEFT is to keep the majority of pre-trained weights frozen while tuning only a minimal number of additional parameters dedicated to the new task. By lightly fine-tuning, these methods aim to preserve the generalization while mitigating overfitting. For instance, ProTrack [41] and ViPT [15] modulate RGB features by introducing trainable auxiliary tokens into attention layers. Similarly, methods like BAT [42] and SDSTrack [16] insert lightweight adapter modules between attention layers for cross-modal shift compensation. More recently, unified trackers like UnTrack [17] and OneTracker [1] employ LoRA and prompt tuning to seamlessly integrate multiple modalities, enabling effective unification across diverse inputs. Despite their effectiveness, excessive constraints on pre-trained weights can incur insufficient adaptation. Furthermore, the added modules tend to over-fit since the additional parameters are optimized from scratch when tailored to modality-specific tasks. Consequently, how to efficiently fine-tune RGB-based pre-trained models for multi-modal tracking remains a significant challenge.

III. PROPOSED METHOD

Learning generalized and coherent representations is crucial for adapting RGB-based models to multi-modal trackers. To unlock the full potential of pre-trained trackers, we revisit the core principles of cross-modal transfer process. In Section III-A, we first present the architectural design of our multi-modal trackers and highlight the key challenges associated with full fine-tuning. Next, in Section III-B, we identify pronounced prior and transfer sensitivities that contribute to catastrophic forgetting and training instability, and further quantify these critical sensitivities. Finally, in Section III-C, we incorporate these sensitivities into the tuning phase, enabling adaptive and dynamic modulation of parameter updates.

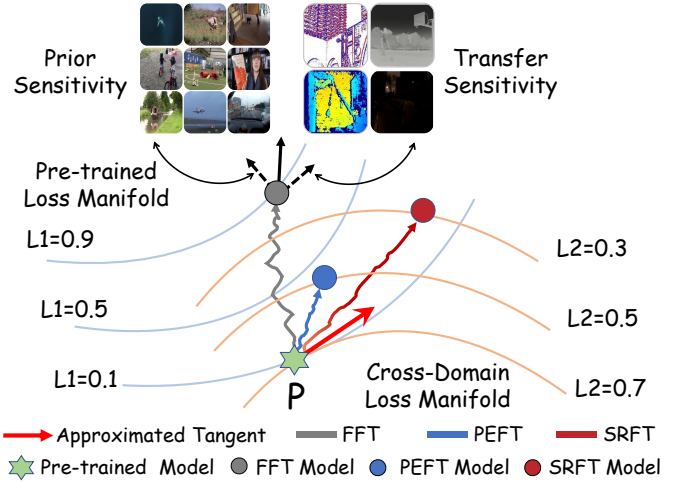


Fig. 3. Loss-parameter manifold schematic for different fine-tuning paradigms. The “FFT” fine-tunes all pre-trained weights without regularization, leading to significant catastrophic forgetting on pre-trained dataset. Although “PEFT”-based methods only tune the additional parameters to maintain the pre-trained knowledge, but their coarse modeling limits performance on new domain. In contrast, our “SRFT” method carefully optimize the model within an approximated tangent space of the pre-trained manifold, indicating a better plasticity-stability trade-off between pre-trained knowledge and adaptation.

A. Preliminaries

Network Architecture. Fig. 2 depicts the overall architecture of our multi-modal tracker. The RGB and auxiliary inputs are first fed to the embedding layer to generate the corresponding tokens. Then, symmetric transformer backbones (e.g., ViT or its variants) handle feature extraction and interaction. Without involving customized multi-modal fusion modules, we repurpose certain ViT blocks for multi-stage fusion of multi-modal tokens. To retain modal-agnostic object association knowledge, the pre-trained box head is utilized and kept frozen.

Cross-Domain Transfer. We consider $f_{\theta}(\cdot) : X \rightarrow Y$ as a multi-modal tracker with parameters $\theta \in \mathbb{R}^{|\theta|}$, with $|\theta|$ representing the total number of the parameter θ . It takes task dataset $D = \{X, Y\} = \{(x_i, y_i)\}_{i=1}^M$ to yield the optimal θ , where x represents a multi-modal input pair and y is the target bounding box. In this paper, we focus on efficiently transferring the models pre-trained on a source domain D_0 (e.g., large-scale RGB data) to downstream domains D_t (e.g., auxiliary modalities or degraded images), where typically $|D_0| \gg |D_t|$. In this setting, let θ_0 be the pre-trained parameters (optimal on D_0), which serve as initialization. After fine-tuning on D_t , the parameters become θ_t . Given a task-specific loss function \mathcal{L} , the **vanilla transfer objective** is:

$$\theta_t = \arg \min_{\theta} \mathcal{L}(\theta | D_t), \quad s.t. \theta^{(0)} = \theta_0, \quad (1)$$

However, directly optimizing θ_t as per Eq. (1) leads to severe catastrophic forgetting and unstable tuning, as evidenced by the pronounced over-fitting and oscillations in training dynamics observed in Fig. 1. This motivates a more principled transfer learning approach described next.

B. Modeling Sensitivity for Multi-Modal Tracking

Effective cross-domain fine-tuning necessitates a delicate balance between stability (preserving critical pre-trained knowledge) and plasticity (adapting to the new domain) [43]. We regulate this trade-off via two intrinsic parameter sensitivities, identifying the evolving parameter importance from pre-trained to target tasks: **prior sensitivity**, reflecting its importance to pre-trained knowledge, and **transfer sensitivity**, indicating its role in target-task adaptation. Excessive changes to highly sensitive parameters in either aspect can hinder the transfer process.

Manifold hypothesis. As shown in Fig. 3, the parameter set $\{\theta\}_{L=L_c}$, with certain loss L_c , does not fill the entire space $\mathbb{R}^{|\theta|}$. Instead, it usually lies in a manifold \mathcal{M}_{L_c} , which is also continuous in $\mathbb{R}^{|\theta|}$.

Based on the aforementioned manifold hypothesis, to avoid the losing of generalization ability for fine-tuned models on downstream domains, the critical thing lies on optimize the model on **local tangent space**, shown as the red arrow of the Fig. 3. Thus, in the following section, we investigate the method to *approximate* and *optimize* the model on such tangent space.

1) **Safeguarding Generalization via Prior Sensitivity:** In this context, we first analyze the influence of the tangent space on model generalization from the pre-trained loss-parameter manifold, and then design an efficient eigen-decomposition method to quantify this sensitivity.

Exploring Parameter Manifold Geometry. We first define the joint empirical risks for tuning models over the union of pre-training and downstream tasks as

$$\mathcal{L}(\theta \mid D_u) = \mathcal{L}(\theta \mid D_t) + \beta \mathcal{L}(\theta \mid D_0), \quad (2)$$

where $D_u = D_0 \cup D_t$, $\beta > 0$ balances the contributions of pre-trained task, and $\mathcal{L}(\theta \mid D_0)$ serves as a regularization term to refine the vanilla objective. Under this joint objective, the pre-trained weights θ_0 minimize $\mathcal{L}(\theta \mid D_0)$ and can serve as a local optimum of $\mathcal{L}(\theta \mid D_u)$. When θ is in the vicinity of θ_0 , the pre-training loss can be locally approximated by a second-order Taylor expansion:

$$\begin{aligned} \mathcal{L}(\theta \mid D_0) &= \mathcal{L}(\theta_0 \mid D_0) + (\theta - \theta_0)^T \nabla \mathcal{L}(\theta_0) + \\ &\quad \frac{1}{2} (\theta - \theta_0)^T \mathcal{F}^{(\theta_0)} (\theta - \theta_0) + \mathcal{O}(\|\theta - \theta_0\|^3), \end{aligned} \quad (3)$$

where $\nabla \mathcal{L}(\theta_0) \approx \mathbf{0}$, and $\mathcal{F}^{(\theta_0)} \in \mathbb{R}^{|\theta| \times |\theta|}$ is expectation of Hessian matrix $\frac{\partial^2 \mathcal{L}}{\partial \theta_i \partial \theta_j}$ over dataset D_0 , also called as the Fisher Information Matrix (FIM) [44] at θ_0 . Principally, it captures the pre-trained tangent space, along which the impact on the pre-trained loss is minimized.

Eq. (3) reveals that the increase in pre-training loss introduced by transferring weights can be interpreted as the generalization gap:

$$\begin{aligned} \varepsilon_{gen} &= \mathcal{L}(\theta \mid D_0) - \mathcal{L}(\theta_0 \mid D_0) \\ &\approx \frac{1}{2} (\theta - \theta_0)^T \mathcal{F}^{(\theta_0)} (\theta - \theta_0) = \frac{1}{2} \|\theta - \theta_0\|_{\mathcal{F}^{(\theta_0)}}^2, \end{aligned} \quad (4)$$

This generalization gap is measured as the weight distance within the Riemannian manifold defined by the FIM. Through

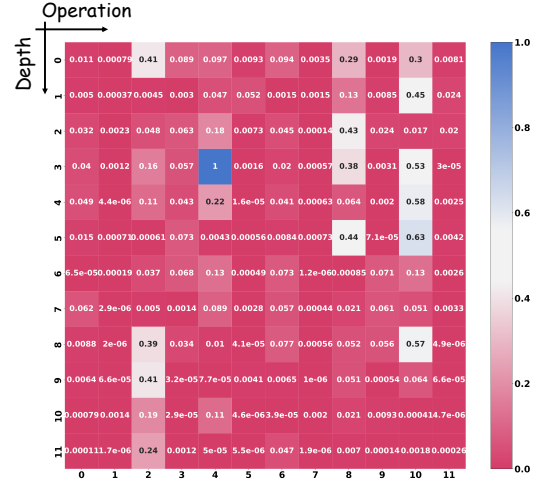


Fig. 4. The operation-wise eigen-decomposition FIM map (i.e., prior sensitivity) of the pre-trained OSTRack. The high prior sensitivity indicates a tendency to deviate from the pre-trained tangent space, reflecting the disruption of pretrained knowledge.

geometric perspective, the FIM yields insights that large deviations from pre-trained tangent space entail a higher risk of generalization degradation [45], [46]. Therefore, the FIM serves as a natural and principled prior sensitivity to reflect the erosion of pre-trained knowledge.

Eigen-decomposition FIM Approximation. Directly computing the FIM for a large model is computationally intractable due to its $\mathcal{O}(|\theta|^2)$ complexity. Instead, we propose constructing an eigen-decomposition approximation of the FIM without explicitly forming it in full. Focusing on leading eigenvalues captures key tangent geometrics of affecting generalization while reducing complexity. Specifically, we partition the model's parameters into N disjoint operation groups, $\theta = \{\theta^1, \dots, \theta^N\}$ (e.g. MLPs of FFNs and attention QKVs). Assuming inter-operation independence, we yield a group-diagonal FIM: $\mathcal{F}^{(\theta_0)} = \text{diag}(\mathcal{F}^{(\theta_0^1)}, \dots, \mathcal{F}^{(\theta_0^N)})$, where $\mathcal{F}^{(\theta_0^j)} \in \mathbb{R}^{|\theta^j| \times |\theta^j|}$ corresponds an independent parameter group j . Parameters from different groups thus span orthogonal subspaces with no second-order coupling.

Empirical studies [47], [48] have shown that the FIM of deep networks are spectrally concentrated, featuring a few large eigenvalues and a long, flat tail, which motivates a low-rank approximation using its leading eigenpairs. Let $\tilde{\mathcal{F}}^{(\theta_0^j)} = (V^j) \Lambda^j (V^j)^T$ be the eigen-decomposition, with unit eigenvectors $V^j = [v_1^j, \dots, v_K^j]$ and eigenvalues $\Lambda^j = \text{diag}(\lambda_1^j, \dots, \lambda_K^j)$ sorted $\lambda_1^j \geq \dots \geq \lambda_K^j \geq 0$.

We obtain these leading eigenpairs via Rayleigh-quotient probing [49]. For any non-zero direction ϵ , the Rayleigh quotient is defined as:

$$\mathcal{R}(\mathcal{F}^{(\theta_0)}, \epsilon) = \frac{\epsilon^T \mathcal{F}^{(\theta_0)} \epsilon}{\epsilon^T \epsilon}, \quad (5)$$

By Rayleigh's theorem, $\mathcal{R}(\mathcal{F}^{(\theta_0)}, \epsilon)$ is maximized when ϵ aligns with the eigenvector corresponding to the largest eigenvalue of $\mathcal{F}^{(\theta_0)}$. Hence, searching for the "most misdirected" tangents is equivalent to finding the dominant eigenpair $(\lambda_{\max}, v_{\max})$, in which case $\lambda_{\max} = \frac{v_{\max}^T \mathcal{F}^{(\theta_0)} v_{\max}}{v_{\max}^T v_{\max}}$.

This formula links the sharpest directions of generalization degradation to the dominant FIM eigenvalues, providing both theoretical motivation and practical guidance.

Proposition 1 (Eigen-based Approximation Error Bound): Let $\tilde{\mathcal{F}}(\theta_0^j) = (V^j)\Lambda^j(V^j)^T$ be the eigen-decomposition of group j , with top- K eigenvalues $\Lambda^j = \text{diag}(\lambda_1^j, \dots, \lambda_K^j)$ and eigenvectors $V^j = [v_1^j, \dots, v_K^j]$. We construct the following approximation:

$$\tilde{\mathcal{F}}(\theta_0^j) = \gamma^j I_{|\theta^j|}, \quad \text{with} \quad \gamma^j = \frac{1}{K} \sum_{i=1}^K \lambda_i^j, \quad (6)$$

where $\tilde{\mathcal{F}}(\theta_0) = \text{diag}(\tilde{\mathcal{F}}(\theta_0^1), \dots, \tilde{\mathcal{F}}(\theta_0^N))$ denotes the approximate group-diagonal low-rank FIM. Then the following guarantees hold:

1. **Bounded FIM Error.** The group-level low-rank approximation $\tilde{\mathcal{F}}(\theta_0)$ captures the principal tangent of $\mathcal{F}(\theta_0)$ with bounded error. In particular, the Frobenius-norm error satisfies: $\|\mathcal{F}(\theta_0) - \tilde{\mathcal{F}}(\theta_0)\|_F \leq \sqrt{\sum_{j=1}^N \sum_{i=K+1}^{|\theta^j|} (\lambda_i^j)^2}$, representing the lost Fisher information. If the top- K eigenvalues dominate, $\tilde{\mathcal{F}}(\theta_0)$ is a close approximation to $\mathcal{F}(\theta_0)$.
2. **Bounded Generalization Gap Error.** For any parameter difference $\Delta\theta \in \mathbb{R}^{|\theta|}$, let $\varepsilon_{\text{gen}}(\mathcal{F}(\theta_0)) = \frac{1}{2} \Delta\theta^T \mathcal{F}(\theta_0) \Delta\theta$ denote the generalization gap induced by the true FIM. Likewise $\varepsilon_{\text{gen}}(\tilde{\mathcal{F}}(\theta_0)) = \frac{1}{2} \Delta\theta^T \tilde{\mathcal{F}}(\theta_0) \Delta\theta$ is the approximated generalization gap. Then the discrepancy between these distances is bounded: $|\varepsilon_{\text{gen}}(\mathcal{F}(\theta_0)) - \varepsilon_{\text{gen}}(\tilde{\mathcal{F}}(\theta_0))| \leq \frac{1}{2} \|\Delta\theta\|^2 (\max_{1 \leq j \leq N} \lambda_1^j)$.

Proof 1: See Appendix.

Prior Sensitivity Measure. Specifically, we estimate large eigenvalues of FIM using symmetric finite-difference probes [50]. Around θ_0 on D_0 , small fixed-radius perturbations expose the directions that maximize the normalized generalization gap, which is equivalent to Rayleigh quotient of FIM. This procedure systematically maps the pre-trained loss landscape to recover the sharpest generalization shifts and identify the most sensitive parameters. For each group θ^j , by sampling various unit directions $\epsilon^j \in \mathbb{R}^{|\theta^j|}$ from an isotropic Gaussian distribution $\epsilon^j \sim \mathcal{N}(\mathbf{0}, I)$ on the weight sphere, we obtain the empirical measures:

$$\begin{aligned} \lambda^j &= \arg \max_{\|\epsilon^j\|_2 = \rho \|\theta_0^j\|_2} \frac{(\epsilon^j)^T \mathcal{F}(\theta_0^j) (\epsilon^j)}{(\epsilon^j)^T (\epsilon^j)} \\ &\approx \arg \max_{\|\epsilon^j\|_2 = \rho \|\theta_0^j\|_2} \frac{\mathcal{L}(\theta_0^j + \epsilon^j) - 2\mathcal{L}(\theta_0^j) + \mathcal{L}(\theta_0^j - \epsilon^j)}{\|\epsilon^j\|_2^2}, \end{aligned} \quad (7)$$

where $\mathcal{L}(\theta_0^j) \triangleq \mathcal{L}(\theta_0^j | D_0)$, $\rho = 1 \times 10^{-5}$ is a noise radius. By repeating this search, we obtain an approximation of the top- K eigenvalues. This measure provides a principled yet tractable perspective to assess how each group of the model affects generalization. By considering the eigenvalue magnitudes from different perturbation directions, we condense the prior sensitivity of the j^{th} operation into a single scalar by distilling its dominant values:

$$s_j^p = \frac{1}{K} \sum_{i=1}^K \lambda_i^j. \quad (8)$$

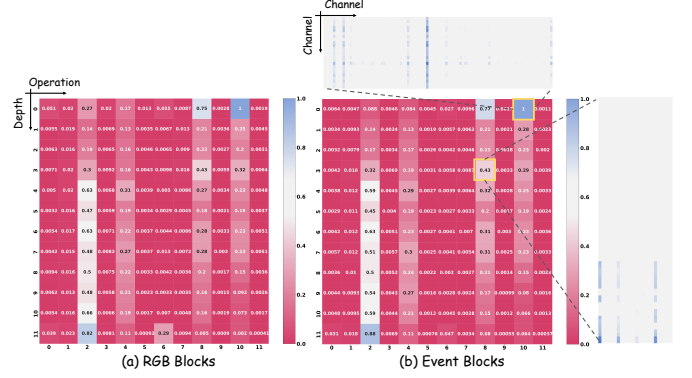


Fig. 5. The instantaneous transfer sensitivity on the VisEvent dataset observed during fine-tuning. The high sparsity in the sensitivity map indicates that only a few gradients (light areas) dominate the updates.

The prior sensitivity is equivalent to FIM in Eq. (6), as presented in Fig. 4. We set $K = 10$ in our experiments. In practice, we observe that the leading eigenvalue alone (e.g., $K = 1$) provides a reliable indicator of prior sensitivity. Further qualitative results are reported in Section IV-C.

2) **Stabilizing Adaptation via Transfer Sensitivity:** In this context, we analyze the impact of sparse transfer gradients on model adaptation and propose rebalancing them using the gradient matrix.

Characterizing Transfer-Gradient Sparsity. While prior sensitivity addresses forgetting of pre-trained domain, inadaptability in the downstream domain is notably pronounced. Multi-modal tracking often involves diverse and heterogeneous samples exhibiting substantial gaps, such as auxiliary inputs or degraded images. These shifts manifest as highly sparse gradients during fine-tuning process on D_t , as illustrated in Fig. 5. High sparsity indicates that only a few gradients dominate the updates, while the majority remain nearly static. This phenomenon sheds light on a key factor underlying the limited adaptability of multi-modal trackers and potentially results in temporal oscillatory (see FFT test branch in Fig. 1). In this context, we investigate the elevated adaptation risk induced by sparse gradients and propose a transfer sensitivity aimed at mitigating its impact.

Formally, we quantify the sparsity of the gradient by comparing its L_1 and L_2 norms. Let $\mathcal{G} \triangleq \nabla_{\theta} \mathcal{L}(\theta | M)$ be the gradient on the current batch $M \subset D_t$. We define the sparsity measure: $\rho = \frac{\|\mathcal{G}\|_1}{\sqrt{|\theta|} \|\mathcal{G}\|_2}$. This definition leverages the fact that L_1 and L_2 norms characterize different aspects of the vector: while L_1 reflects the total variation, L_2 emphasizes concentration [51]. Thus, their ratio serves as an effective proxy for sparsity structure, where a smaller value means higher sparsity. Moreover, noting that single-step gradient magnitudes are typically bounded [52], increasing sparsity (i.e., $\rho : 1 \rightarrow \frac{1}{\sqrt{|\theta|}}$) can amplify the L_2 norm:

$$\|\mathcal{G}\|_2 = \frac{\|\mathcal{G}\|_1}{\rho \sqrt{|\theta|}}. \quad (9)$$

Sparsity-Induced Adaptation Risk. We characterize the tuning volatility as the degree to which performance responds to

small parameter perturbations during fine-tuning. Accordingly, we define the following sensitivity function:

$$S(\theta, \delta | M) = \mathcal{L}(\theta | M) - \mathcal{L}(\theta + \delta | M), \quad (10)$$

where δ is a random perturbation centered on the current update step, i.e., $\delta \sim \mathcal{N}(\alpha \mathcal{G}, \sigma^2 I)$, α is the learning rate and σ controls the noise. This denotes that updates follow the gradient with inherent noise (due to stochastic sampling, batch gap, etc.).

Intuitively, a smooth and stable loss landscape should ensure that varying perturbations yield consistent responses. The expected magnitude of this difference defines the adaptation risk:

$$\varepsilon_{ada} = \mathbb{E}_{(\delta, \delta')} [|S(\theta, \delta | M) - S(\theta, \delta' | M)|]. \quad (11)$$

By incorporating the linear approximation $S(\theta, \delta | M) \approx \mathcal{G}^T \delta$ into Eq. (11), it can be shown that this risk is proportional to the L_2 norm of gradient:

$$\varepsilon_{ada} \approx \alpha \sqrt{2\sigma^2} \|\mathcal{G}\|_2. \quad (12)$$

Thus, we can deduce that sparse gradients exacerbate tuning instability and adaptation risk. This highlights the need to avoid concentrating updates on specific parameters and emphasizes the importance of a balanced transfer gradient.

Transfer Sensitivity Estimation. To formalize the estimation of transfer sensitivity, we adapt the formulation of Eq. (10) to the standard tuning process. In this case, we adjust the parameter θ via the gradient \mathcal{G} rather than noise perturbations. Therefore, we can derive: $S(\theta, \delta | M) \approx \mathcal{G}^T \mathcal{G}$. Here, the sensitivity function is used to assess the overall adjustment of all parameters during transfer. To further investigate and regularize gradients, we extend the sensitivity to a parameter-wise formulation:

$$s_n^t = \left(\frac{\partial \mathcal{L}(\theta | M)}{\partial \theta_n} \right)^2, \quad (13)$$

where s_n^t denotes the transfer sensitivity of the n^{th} parameter. This formulation allows us to examine the granular impact of parameter changes during the transfer process and rebalance the gradient accordingly.

C. Sensitivity-Aware Regularization Tuning

We regularize the learning process by previously discussed sensitivity metrics to derive enhanced trackers. To align with the unified regularization tuning, we rank both the operation-wise prior sensitivity and parameter-wise transfer sensitivity, and then normalize them within the continuous range of $[0, 1]$. To harmonize these two sensitivities, we devise a dynamic linear schedule to adjust their weighted combination. At the beginning of training, prior sensitivity plays a dominant role, contributing a weight of κ (where $\kappa \in [0, 1]$). As training progresses, the influence of transfer sensitivity gradually increases, reaching the same weight κ by the end. This ensures that the model initially focuses on retaining pre-trained knowledge and progressively shifts to emphasize training stability.

Algorithm 1: Sensitivity-Aware Regularization Tuning

Input: pre-trained dataset D_0 , downstream task dataset D_t , pre-trained weight θ_0 ; number of eigenvalues K , number of model operations N , training steps T ; initialized eigenvalue set Λ ;

Output: Optimal multi-modal tracker parameters θ_t ;

Step1: Prior Sensitivity Estimation:

for batch (x, y) in D_0 **do**

for $j \in \{1, \dots, N\}$ **do**

 Sample $\epsilon^j \sim \mathcal{N}(\mathbf{0}, I)$;

 Calculate λ^j via Eq. (7);

 Update eigenvalue set Λ for top- K λ^j ;

end for

end for

Calculate prior sensitivity s_j^p via Eq. (8);

Step2: Transfer Sensitivity Estimation and Regularized Tuning:

for $i \in \{1, \dots, T\}$ **do**

 Sample i -th batch data M_i from D_t ;

 Compute loss $\mathcal{L}(\theta | M_i)$ and gradients;

 Update transfer sensitivity by $s_n^t = \left(\frac{\partial \mathcal{L}(\theta | M_i)}{\partial \theta_n} \right)^2$;

 Normalize and combine sensitivity s_n by Eq. (14);

 Parameter update via Eq. (15);

end for

Formally, at each training step t , the combined sensitivity is updated as follows:

$$s_n = (\kappa + (1 - 2\kappa) \frac{t}{T}) s_j^p + (1 - \kappa - (1 - 2\kappa) \frac{t}{T}) s_n^t, \quad (14)$$

where $\theta_n \in \theta^j$, T is the total number of training steps. Finally, we normalize this joint sensitivity within the range of $s_n \in [0, 0.99]$. To this end, during the training process, parameters that are excessively updated will be penalized based on their sensitivity:

$$\theta_n^{(i+1)} = \theta_n^{(i)} - (1 - s_n) \alpha \frac{\partial \mathcal{L}}{\partial \theta_n}, \text{ s.t. } \theta^{(0)} = \theta_0, \quad (15)$$

where α is the learning rate. This formulation suggests that more sensitive parameters should retain their previous states to a greater extent, to avoid oscillations or over-adjustments. The detailed regularization tuning process is given in Algorithm.1. We set the sensitivity harmony coefficient $\kappa = 0.6$ in our experiments. Further comprehensive analysis can be found in Tab. VI.

D. Learning Objectives

The overall loss function of our method is the same as the foundation model without extra adjustments, shown as:

$$\mathcal{L} = \mathcal{L}_{cls} + \lambda_{iou} \mathcal{L}_{iou} + \lambda_{l_1} \mathcal{L}_1, \quad (16)$$

where \mathcal{L}_{cls} is the weighted focal loss for classification, L_1 loss \mathcal{L}_1 and GIoU loss \mathcal{L}_{iou} are employed for bounding box regression, $\lambda_{iou} = 2$ and $\lambda_{l_1} = 5$ are the regularization factors, and all the corresponding settings are the same as [5].

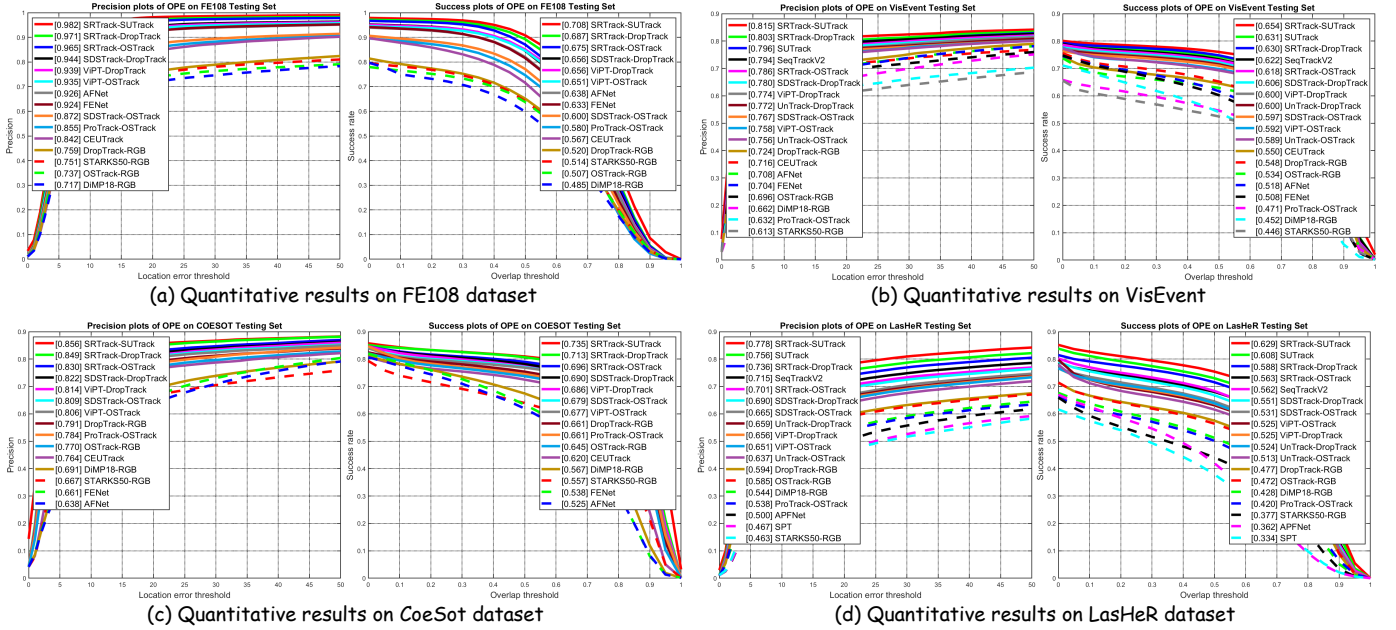


Fig. 6. Visualization of the precision and success plots of the FE108, VisEvent, CoeSot and LasHeR datasets. Zoom in to see details.

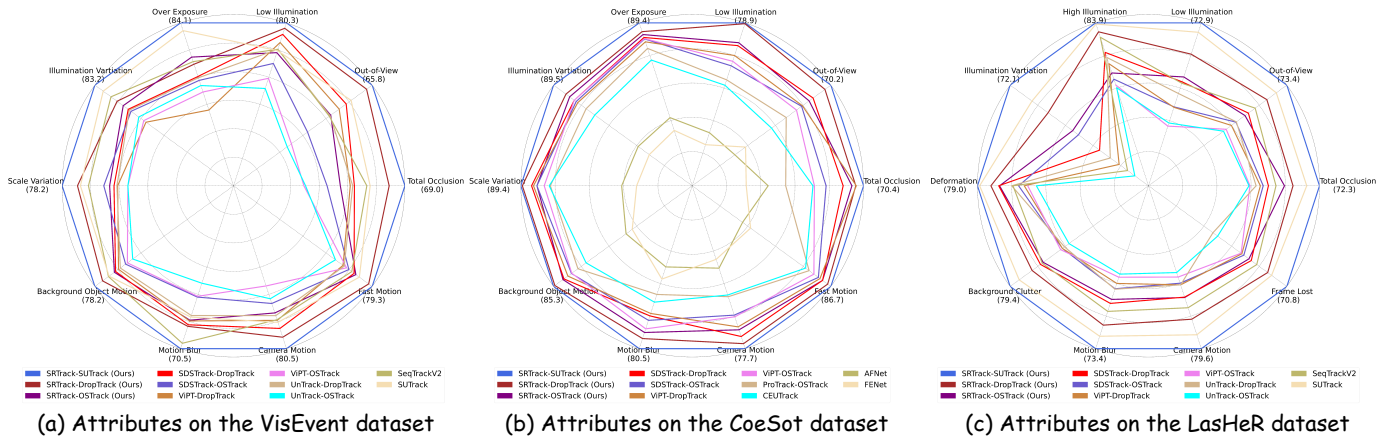


Fig. 7. Precision scores of different attributes on the VisEvent, CoeSot and LasHeR test sets. Zoom in to see details.

IV. EXPERIMENTS

A. Experimental Settings

1) *Benchmark Datasets*: To verify the effectiveness and generalization of the proposed method, we conduct comprehensive experiments on seven multi-modal benchmark datasets. For **RGB-Event** tracking, we use FE108 [53] (76 train / 32 test sequences) captured under degraded conditions, VisEvent [9] (500 train / 320 test sequences) covering dynamic outdoor scenes, and CoeSot [37] with 578K image-event pairs (824 train / 528 test sequences). For **RGB-Depth** tracking, we adopt DepthTrack [31] (152 train / 50 test videos) and VOT-RGBD2022 [54] (127 test sequences). For **RGB-Thermal** tracking, we use LasHeR [55] (979 train / 245 test sequences) and RGBT234 [56] (234 test videos). All training and evaluation strictly follow established protocols [15], [17]. During fine-tuning, we use the training sets of FE108, VisEvent, and CoeSot for RGB-Event tasks; DepthTrack for RGB-Depth; and

LasHeR for RGB-Thermal. The corresponding test sets, along with VOT-RGBD2022 and RGBT234, are used for evaluation.

2) *Evaluation Metrics*: Adhering to recognized standards [1], [11], [16], [17], we evaluated tracking performance with following metrics. For all RGB-Event benchmarks (FE108, VisEvent and CoeSot), We utilize two widely used metrics, i.e., success rate (SR), precision rate (PR). For DepthTrack, precision (Pr) and recall (Re) are used, with F-score ($F = \frac{2Re \cdot Pr}{Re + Pr}$) as the primary measure. For VOT-RGBD2022, we assess accuracy (Acc), robustness (Rob), and expected average overlap (EAO). For LasHeR, success rate (SR) and precision rate (PR) are employed. For RGBT234, maximum success rate (MSR) and maximum precision rate (MPR) served as evaluation metrics. Notably, our SR/PR precisely aligns with SR/PR in ViPT and OneTrack, Suc/Pre in SDSTrack, Success/Precision in UnTrack, or AUC/P in SUTrack. For all metrics, the **larger**, the **better**.

TABLE I
QUANTITATIVE COMPARISON ON THE RGB-EVENT DATASETS. THE BEST ARE MARKED WITH “**BOLD**”, AND THE SECOND BEST ARE MARKED WITH “UNDERLINE”.

Method	Reference	Base Model	FE108		VisEvent		CoeSot	
			SR	PR	SR	PR	SR	PR
Image-based Methods (Only-RGB)								
DiMP [59]	ICCV’19	ResNet	48.5	71.7	45.2	66.2	56.7	69.1
Stark-S [60]	ICCV’21	ResNet	51.4	75.1	44.6	61.3	55.7	66.7
OSTrack [5]	ECCV’22	OSTrack-256	50.7	73.7	53.4	69.6	64.5	77.0
DropTrack [40]	CVPR’23	DropTrack-384	52.0	75.9	54.8	72.4	66.1	79.1
Cross-modal Transfer Learning								
FENet [53]	ICCV’21	DiMP	63.3	92.4	50.8	70.4	53.8	66.1
AFNet [61]	CVPR’23	DiMP	63.8	92.6	51.8	70.8	52.5	63.8
CEUTrack [37]	Arxiv’22	OSTrack-B256	56.7	84.2	55.0	71.6	62.0	76.4
ProTrack [41]	ACM MM’22	OSTrack-B256	58.0	85.5	47.1	63.2	66.1	78.4
HRTrack [10]	ICCV’23	OSTrack-B256	-	-	-	-	63.2	71.9
ViPT [15]	CVPR’23	OSTrack-B256	<u>65.1</u>	<u>93.5</u>	59.2	75.8	67.7	80.6
SDSTrack [16]	CVPR’24	OSTrack-B256	60.0	87.2	<u>59.7</u>	<u>76.7</u>	<u>67.9</u>	<u>80.9</u>
UnTrack [17]	CVPR’24	OSTrack-B256	-	-	58.9	75.6	-	-
Ours	-	OSTrack-B256	67.5	96.5	61.8	78.6	69.6	83.0
ViPT [15]	CVPR’23	DropTrack-B384	65.6	93.9	60.0	77.4	68.6	81.4
SDSTrack [16]	CVPR’24	DropTrack-B384	<u>65.6</u>	<u>94.4</u>	<u>60.6</u>	<u>78.0</u>	<u>69.0</u>	<u>82.2</u>
UnTrack [17]	CVPR’24	DropTrack-B384	-	-	60.0	77.2	-	-
Ours	-	DropTrack-B384	68.7	97.1	63.0	80.3	71.3	84.9
MamTrack [11]	CVPR’25	HiViT-B384	<u>66.4</u>	<u>94.2</u>	61.6	79.2	-	-
SUTrack [8]	AAAI’25	SUTrack-B384	-	-	<u>63.1</u>	<u>79.6</u>	-	-
Ours	-	SUTrack-B384	70.8	98.2	65.4	81.5	73.5	85.6

3) *Pre-trained Models and Compared Methods*: In this paper, we choose three prototypical one-stream RGB-based trackers as pre-trained baselines: OSTRack [5], the most widely adopted model; DropTrack [40] and SUTrack [8], which offer improved generalization. Notably, OSTRack and DropTrack are built upon ViT-B/16 [57], while SUTrack adopts the HiViT-B/16 [58] as the backbone. Following their pre-trained configurations, these models differ in input resolution: OSTRack ($128 \times 128 / 256 \times 256$), DropTrack and SUTrack ($192 \times 192 / 384 \times 384$) for template and search regions, respectively. To comprehensively validate the effectiveness of our method, we conduct the following experiments in Tab. I and Tab. II. First, we construct strong RGB-based single-modal baselines under full fine-tuning. Then, we evaluate our method under both full and parameter-efficient fine-tuning paradigms. For fair comparison, all methods are grouped according to the pre-trained trackers. **Notably**, OneTracker [1] and MamTrack [11] adopt non-standard experimental settings and lack open-source implementations. OneTracker uses a 384×384 pre-trained OSTRack, incompatible with standard benchmarks, so we compare it separately in Tab. III. MamTrack, with unclear pretraining details but sharing the HiViT-B/16 backbone with SUTrack, is included in SUTrack-based comparisons.

4) *Training Details*: We follow the data processing pipeline of SDSTrack [16] across all datasets, converting event data into color-polar event images, with no preprocessing for other auxiliary modalities. The models are trained on 8 NVIDIA 3090Ti GPUs with a batch size of 192 and 30 epochs. Each epoch involves sampling 80k samples. We utilize the AdamW

optimizer with a learning rate set to 1×10^{-4} and a weight decay set to 10^{-4} .

B. Comparison with State-of-the-Art Methods

Extensive comparative analyses are presented in Tab. I, Tab. II and Tab. III, where our method demonstrates excellent performance on all multi-modal benchmarks after incorporating the proposed regularized tuning strategies. The corresponding precision and success plots are illustrated in Fig. 6, further substantiating the quantitative results. Evidently, we can observe that both the RGB-only and the cross-modal trackers are becoming increasingly profitable with pre-trained models. In particular, cross-modal approaches exhibit substantial performance gains, highlighting the complementarity between RGB and auxiliary data under complex conditions. Crucially, the remarkable improvements achieved by our method suggest the significance and necessity of developing tailored cross-domain transfer techniques for multi-modal object tracking.

Results on RGB-Event Tracking. As shown in Tab. I and Tab. III, our method surpasses all state-of-the-art trackers across all RGB-Event datasets, achieving the highest precision scores of 98.2%, 81.5% and 85.6% on the FE108, VisEvent, and CoeSot datasets, respectively. In particular, on FE108, a dataset characterized by low-light conditions and heavy reliance on event information, our approach surpasses the previous best by a notable margin: +3.0% in PR and +2.4% in SR over OSTRack-B256. The full fine-tuning approaches (e.g., CEUTrack, MamTrack) yield limited improvements,

TABLE II
QUANTITATIVE COMPARISON ON THE RGB-DEPTH AND RGB-THERMAL DATASETS. THE BEST ARE MARKED WITH “**BOLD**”, AND THE SECOND BEST ARE MARKED WITH “UNDERLINE”.

Method	Reference	Base Model	DepthTrack			VOT RGBD2022			LasHeR		RGBT234	
			Pr	Re	F-score	Acc	Rob	EAO	SR	PR	MSR	MPR
Image-based Methods (Only-RGB)												
DiMP [59]	ICCV’19	ResNet	46.3	42.8	44.5	70.3	73.1	54.3	42.8	54.4	42.1	62.5
Stark-S [60]	ICCV’21	ResNet	39.3	37.6	38.4	65.4	62.8	48.2	37.7	46.3	48.9	66.5
OSTrack [5]	ECCV’22	OSTrack-B256	53.6	52.2	52.9	80.3	83.3	67.6	47.2	58.5	54.9	72.9
DropTrack [40]	CVPR’23	DropTrack-B384	56.4	55.8	56.1	81.5	85.1	69.2	47.7	59.4	57.2	75.8
Cross-modal Transfer Learning												
SPT [62]	AAAI’23	Stark-S	52.7	54.9	53.8	79.8	85.1	65.1	33.4	46.7	55.5	78.6
APFNet [63]	AAAI’22	Stark-S	51.6	51.4	51.5	79.0	83.7	64.2	36.2	50.0	57.9	82.7
ProTrack [41]	ACM MM’22	OSTrack-B256	58.3	57.3	57.8	80.1	80.2	65.1	42.0	53.8	59.9	79.5
ViPT [15]	CVPR’23	OSTrack-B256	59.2	59.6	59.4	81.5	87.1	72.1	52.5	65.1	61.7	83.5
SDSTrack [16]	CVPR’24	OSTrack-B256	61.9	60.9	61.4	81.2	88.3	72.8	53.1	66.5	62.5	84.8
UnTrack [17]	CVPR’24	OSTrack-B256	61.1	60.8	61.0	82.0	86.9	72.1	51.3	63.7	62.5	84.2
Ours	-	OSTrack-B256	64.7	65.4	65.1	82.1	88.8	74.1	56.3	70.1	64.4	87.2
ViPT [15]	CVPR’23	DropTrack-B384	62.6	61.9	62.2	81.7	87.3	72.3	52.5	65.6	63.4	84.7
SDSTrack [16]	CVPR’24	DropTrack-B384	63.3	62.2	62.7	81.4	88.6	73.0	55.1	69.0	65.0	87.1
UnTrack [17]	CVPR’24	DropTrack-B384	62.4	61.7	62.0	82.1	87.1	72.2	52.4	65.9	64.1	85.2
Ours	-	DropTrack-B384	67.2	67.1	67.1	82.9	89.2	74.5	58.8	73.6	66.7	89.1
MamTrack [11]	CVPR’25	HiViT-B384	-	-	-	-	-	-	54.2	67.4	62.4	84.4
SUTrack [8]	AAAI’25	SUTrack-B384	58.8	58.6	58.7	83.0	90.6	75.4	60.8	75.6	69.2	92.1
Ours	-	SUTrack-B384	65.1	65.2	65.2	84.1	92.6	77.7	62.9	77.8	70.3	93.3

TABLE III
QUANTITATIVE COMPARISON WITH ONETRACKER.

Method	Reference	Base Model	VisEvent		DepthTrack			VOT RGBD2022			LasHeR		RGBT234	
			SR	PR	Pr	Re	F-score	Acc	Rob	EAO	SR	PR	MSR	MPR
OneTracker [1]	CVPR’24	OSTrack-B384	60.8	76.7	60.7	60.4	60.9	81.9	87.2	72.7	53.8	67.2	64.2	85.7
Ours	-	OSTrack-B384	62.6	79.4	65.3	66.1	65.6	82.4	88.9	74.3	57.0	71.2	65.4	87.9

while parameter-efficient fine-tuning paradigms (e.g., ViPT, SDSTrack) face performance bottlenecks. This stems from a misfit that impedes cross-modal transfer, emphasizing the effectiveness of our regularized tuning.

Results on RGB-Depth Tracking. As depicted in Tab. II and Tab. III, our method outperforms all previous state-of-the-art trackers on DepthTrack, obtaining the top performance 67.1% in F-score. Using the pre-trained OSTrack-B256, our method yields substantial improvements: +2.8% in Pr, +4.5% in Re, and +3.7% in F-score. Similarly, when built on the DropTrack-B384 with richer pre-trained knowledge, our method demonstrates superior performance gains, +3.9% in Pr, +4.9% in Re, and +4.4% in F-score. Furthermore, despite no training on the VOT-RGBD2022 dataset, our method still delivers enhanced performance with a +2.3% gain in EAO over existing baselines. This clearly demonstrates the strong generalization and transferability of our approach in cross-modal tracking scenarios.

Results on RGB-Thermal Tracking. As listed in Tab. II and Tab. III, our method achieves 70.1% precision and 56.3% success when evaluated on the pre-trained OSTrack-B256. Furthermore, our method effectively unleashes the potential of the DropTrack, yielding substantial improvements of +4.6%

in PR, +3.7% in SR. Remarkably, with SUTrack as our pre-trained baseline, our method sets a new state-of-the-art, reaching 77.8% in PR and 62.9% in SR. Beyond the established benchmarks, our method also excels on the unseen RGBT234 dataset, attaining 93.3% MPR and 70.3% MSR. These results not only underscore the superior performance of our method but also validate its exceptional cross-dataset generalization capabilities.

Attribute Analysis. To comprehensively analyze our method, we present a detailed per-attribute comparison in Fig. 7. Our approach consistently achieves the best performance across nearly all challenging attributes while significantly leading. Specifically, for motion-related sequences from the VisEvent and CoeSot datasets, our method delivers the best results, highlighting strong robustness against motion-induced degradation. Particularly, it yields precision gains of +5.6% under Motion Blur, +3.0% under Camera Motion. On the LasHeR, our regularization strategy yields notable improvements under extreme lighting conditions: +13.4% under Illumination Variation, +6.2% under Low Illumination, and +5.3% under Over Exposure. Moreover, our method also maintains superior performance across other challenging attributes such as Out-of-View and Frame Lost.

TABLE IV

ABLATIVE STUDY RESULTS OF THE PROPOSED KEY COMPONENTS. “FFT” REFERS TO FULL FINE-TUNING OF THE BACKBONE; (A) IS THE ZERO-SHOT PERFORMANCE; (B) SERVES AS OUR BASELINES; (E) DENOTES THE COMPLETE REGULARIZED TUNING FRAMEWORK.

Exp.	FFT	Prior Sensitivity	Transfer Sensitivity	FE108		DepthTrack			LasHeR	
				SR	PR	Pr	Re	F-score	SR	PR
(a)				48.8	75.2	38.2	36.0	37.1	36.7	43.5
(b)	✓			65.2	93.5	61.6	61.4	61.5	53.2	65.8
(c)	✓	✓		66.8	95.4	64.1	64.5	64.3	55.6	69.0
(d)	✓		✓	66.6	94.9	63.9	64.2	64.1	55.1	68.4
(e)	✓	✓	✓	67.4	96.5	64.7	65.4	65.1	56.3	70.1

C. Ablation Study and Analysis

We conducted ablative analyses to verify the effectiveness and characteristics of sensitivity-aware regularization tuning. In the ablation section, “full fine-tuning” refers to training the entire backbone, excluding the box head (as Section III-A). All methods use the pre-trained OSTRack-B256 weights unless otherwise specified.

Effectiveness of Proposed Sensitivities. We conduct a series of comprehensive experiments to uncover the interplay and effectiveness of the two proposed sensitivity items, as summarized in Tab. IV. A comparison of (a) and (b) demonstrates that fine-tuning significantly enhances the domain adaptation ability. Further, the contrast between (b) and (c) (or (d) and (e)) figures out that the prior sensitivity regularization scheme significantly improves SR by +2.4% and PR by +3.2% on LasHeR, highlighting its effectiveness. Similarly, the comparison between (b) and (d) (or (c) and (e)) reveals that rebalancing gradients optimized with diverse transfer data leads to substantial improvements. Notably, the simultaneous application of both prior and transfer sensitivity yields significantly greater improvements than either method alone, proving their complementary nature. While the transfer sensitivity penalty alone yields only modest improvement on FE108, it still contributes to the overall leading performance of our method.

Eigenvalue Budget (Top- K) for Prior Sensitivity. In this section, we examine the effect of the low-dimension eigenvalue count K in Eq. (8). For each operation, we record up to the 20 largest eigenvalues during Rayleigh-quotient probing and compute the prior sensitivity using the top- K of them. As shown in Tab. V, decreasing K from 20 to 1 has little impact: $K = 5$ performs on par with $K = 10$ (the best configuration), and even $K = 1$ still yields a clear improvement over the baseline. This indicates that the effectiveness of our regularizer depends primarily on the relative ranking of sensitivities rather than their absolute magnitudes. Under our low-dimension approximation, the central challenge lies in accurately identifying the operations most sensitive to the generalization gap.

Settings of Sensitivity Harmony Coefficient κ . In this section, we evaluate the impact of different sensitivity harmony coefficients, κ as defined in Eq. (14), with the detailed results presented in Tab. VI. By systematically increasing κ from 0.1 to 0.9, we observe that a moderately large coefficient (e.g., 0.6) yields the best performance, outperforming both smaller (e.g., 0.3) and larger values (e.g., 0.9). This finding suggests that while both prior sensitivity and transfer sensitivity contribute to performance improvements from different perspectives, a

TABLE V

ABLATION ANALYSIS OF LOW-DIMENSION EIGENVALUE COUNT K ON PRIOR SENSITIVITY ESTIMATION.

Exp.	FE108		DepthTrack			LasHeR	
	SR	PR	Pr	Re	F-score	SR	PR
$K=1$	66.5	95.0	63.9	64.3	64.1	55.2	68.7
$K=2$	66.6	95.2	64.0	64.4	64.2	55.4	68.8
$K=5$	66.8	95.3	64.1	64.4	64.2	55.5	69.0
$K=10$	66.8	95.4	64.1	64.5	64.3	55.6	69.0
$K=20$	66.4	95.2	64.1	64.4	64.2	55.4	68.9

TABLE VI

ABLATION ANALYSIS OF SENSITIVITY HARMONY COEFFICIENT ON THE FE108 DATASET.

κ	0.1	0.2	0.3	0.4	0.5	0.6	0.7	0.8	0.9
SR	66.5	66.7	66.9	66.9	67.2	67.4	67.1	66.8	66.9
PR	94.7	94.8	95.1	95.3	96.0	96.5	96.2	95.8	95.5

delicate balance between them further optimizes the fine-tuning process, promoting better generalization and adaptability.

Impact of Box Head Tuning. In our default setting, “full fine-tuning” updates the backbone while keeping the box head frozen. To assess the impact of tuning the box head, we also examine a more aggressive variant, complete fine-tuning, where the box head is updated as well. As shown in Tab. VII, unfreezing the box head further exacerbates over-fitting. While our regularization method remains effective, the results reveal an important caveat: unfreezing the box head during cross-modal adaptation can be risky, as it tends to disrupt the modal-agnostic object association knowledge encoded during pre-training.

Compatibility with PEFT Methods. Existing PEFT methods [15]–[17] typically freeze pre-trained parameters and update only a minimal number of additional parameters, which can hinder sufficient optimization. To evaluate the compatibility of our proposed regularization techniques with these methods, we unfreeze their backbones and retrain them with our regularization applied. As shown in Tab. VIII, our approach significantly enhances ViPT’s performance on ViSEvent, yielding gains of +2.1% in SR and +2.0% in PR. Notably, even for the unified tracker UnTrack, our approach achieves superior results on LasHeR: +2.7% in SR and +3.7% in PR. This demonstrates that overly rigid constraints on pre-trained models limit their transfer potential. However, our method negatively impacts SDSTrack, likely because it optimizes the pre-trained parameters, whereas SDSTrack relies

TABLE VII

ABLATION RESULTS OF BOX HEAD TUNING. “**Box**” DENOTES TUNING THE BOX HEAD, “**S-Reg**” REPRESENTS THE SENSITIVITY-AWARE REGULARIZATION TUNING METHOD.

Exp.	Box	FE108		DepthTrack			LasHeR	
		SR	PR	Pr	Re	F-score	SR	PR
FFT	w/	63.8	91.0	59.4	58.7	59.0	51.5	64.4
FFT	w/o	65.2	93.5	61.6	61.4	61.5	53.2	65.8
FFT+S-Reg	w/	66.2	95.3	62.6	63.4	63.0	54.4	67.7
FFT+S-Reg	w/o	67.4	96.5	64.7	65.4	65.1	56.3	70.1

TABLE VIII

COMPATIBILITY STUDY RESULTS OF THE PROPOSED REGULARIZATION TUNING METHOD ON EXISTING PEFT METHODS. “**FFT**” DENOTES FULL FINE-TUNING OF THE BACKBONE, WHILE “**S-Reg**” REPRESENTS THE SENSITIVITY-AWARE REGULARIZATION TUNING SCHEME.

Exp.	VisEvent		DepthTrack			LasHeR	
	SR	PR	Pr	Re	F-score	SR	PR
ViPT	59.2	75.8	59.2	59.6	59.4	52.5	65.1
ViPT+FFT	57.5	74.0	58.2	57.4	57.8	50.9	63.8
ViPT+FFT+S-Reg	61.3	77.8	61.9	61.4	61.6	54.9	68.4
UnTrack	58.9	75.6	61.1	60.8	61.0	51.3	63.7
UnTrack+FFT	56.6	73.1	58.2	56.8	57.5	48.1	60.2
UnTrack+FFT+S-Reg	60.2	76.9	61.9	62.5	62.2	54.0	67.4
SDSTrack	59.7	76.7	61.9	60.9	61.4	53.1	66.5
SDSTrack+FFT	56.0	72.0	57.8	56.4	57.1	50.7	63.8
SDSTrack+FFT+S-Reg	57.8	74.8	59.5	58.3	58.9	52.5	65.8
Ours	61.8	78.6	64.7	65.4	65.1	56.3	70.1

on modal-specific adapters trained from scratch.

Compatibility with Single-modality Methods. This work aims to mitigate the misfitting issue when adapting the foundation trackers to downstream tasks. A central question is how the proposed regularization methods perform on single-modality data. To investigate this, we conduct ablation studies highlighting their impact on different modalities. As shown in Tab. IX, both RGB and auxiliary modalities benefit significantly from our regularization techniques. For example, the RGB and depth modalities achieve F-score gains of +5.3% and +4.0%, respectively, on the DepthTrack dataset. Despite substantial distribution differences, our method significantly and consistently enhances the adaptability of auxiliary modalities across various tasks. These findings underscore the importance and necessity of applying constraints when transferring the pre-trained trackers to downstream domains.

Impact of Event Representations. In this work, we focus on constructing suitable frame-like event representations tailored to cross-modal transfer. In this experiment, we keep the same training setup, varying only the input event representations. As shown in Tab. X, surface-based representations (TSLTD, Time Surface) perform poorly, likely due to the randomness of event timestamps. In contrast, count-based representations (Event Count, Event Frame) offer more robust performance. The time-interpolation-based Event Volume further improves results by utilizing time-weighted and multi-channel methods to preserve spatio-temporal information. Notably, we employ simple color-polarity event images (with ViPT) to align with the RGB pre-trained model, leading to superior performance.

Effectiveness of Smaller Learning Rates. In this paper, we exploit the sensitivity-regularized gradients to bolster the

TABLE IX

COMPATIBILITY STUDY RESULTS OF THE PROPOSED REGULARIZATION TUNING METHOD ON SINGLE-MODAL DATA. “**S-Reg**” REPRESENTS THE REGULARIZATION TUNING METHOD.

Exp.	CoeSot		DepthTrack			LasHeR	
	SR	PR	Pr	Re	F-score	SR	PR
RGB	64.3	76.3	53.9	53.0	53.4	47.2	58.6
RGB+S-Reg	68.0	80.0	58.8	58.6	58.7	50.3	62.6
Auxiliary	57.5	69.8	49.0	47.3	48.1	42.7	53.7
Auxiliary+S-Reg	60.5	73.7	52.9	51.3	52.1	45.9	57.8

TABLE X

ABLATION RESULTS OF DIFFERENT EVENT REPRESENTATIONS.

Exp.	FE108		VisEvent		CoeSot	
	SR	PR	SR	PR	SR	PR
Event Frame [64]	66.8	95.5	61.2	77.6	68.8	82.0
Event Count [65]	66.3	95.1	59.8	76.9	67.9	81.2
Time Surface [66]	66.1	94.9	60.3	77.1	67.4	80.6
TSLTD [67]	66.5	95.2	61.0	77.4	67.9	81.3
Event Volume [68]	67.3	96.1	61.4	77.9	69.1	82.4
Color-Polar Event Image (Ours)	67.5	96.5	61.8	78.6	69.6	83.0

transfer process. A straightforward strategy might involve using a smaller learning rate. To investigate this, we evaluate the effect of reduced learning rates. As shown in Tab. XI, a smaller learning rate (i.e., $\alpha = 10^{-5}$) yields negligible improvement in PR, but at the cost of a decline in SR. Further reduction (i.e., $\alpha = 10^{-6}$) leads to overall performance degradation. These findings suggest that merely reducing the learning rate is insufficient to address over-fitting in cross-modality adaptation, while simultaneously limiting transfer potential, as it uniformly suppresses parameter updates without prioritizing those that are sensitive or high-risk.

TABLE XI

ABLATION ANALYSIS OF SMALLER LEARNING RATES α ON THE LASHER DATASET.

Exp.	SR	PR
$\alpha = 10^{-4}$	53.2	65.8
$\alpha = 10^{-5}$	52.9	66.2
$\alpha = 10^{-6}$	52.5	65.4
Ours	56.3	70.1

Observations on Weight Variations. To intuitively demonstrate the effectiveness of the proposed sensitivity-aware regularization tuning, we visualize parameter dynamics during training from both spatial and temporal perspectives, as depicted in Fig. 8 and Fig. 9. Overall, our regularization encourages smaller and more evenly distributed weight deviations, effectively mitigating over-fitting and facilitating stable adaptation. As shown in Fig. 8, for parameters with high prior sensitivity, such as `blocks.3.attn.proj.weight` (highlighted in the orange box), our method effectively suppresses excessive updates. As further demonstrated in Fig. 9, our method facilitates faster convergence and achieves a substantial reduction in sensitivity-weighted weight deviations (e.g., up to 80%), indicating improved retention of the pre-trained knowledge while ensuring desired task adaptation. Moreover, the vanilla fine-tuning causes parameter updates

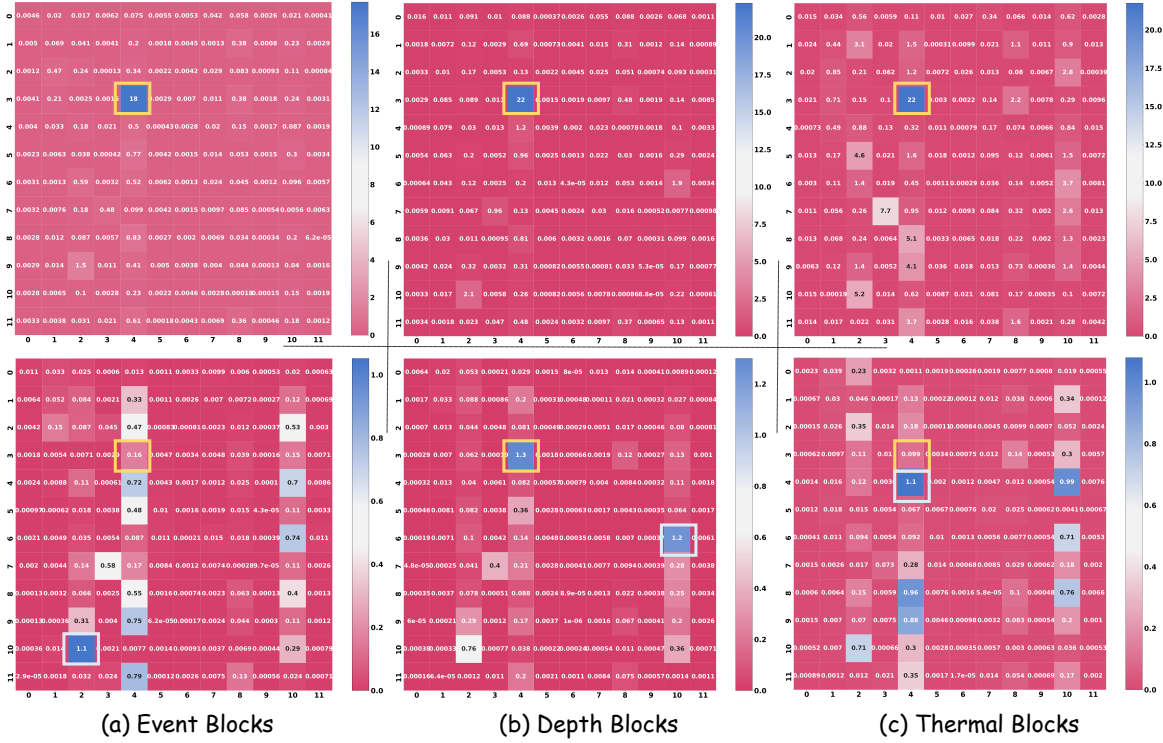


Fig. 8. Operation-wise weight distances $\frac{\|\theta_t - \theta_0\|_2}{\|\theta_0\|_2}$ between the tuned model and the pre-trained model after training, including results from vanilla full fine-tuning (**upper**) and our regularized tuning (**bottom**). The auxiliary branches are derived from the VisEvent, DepthTrack, and LasHer datasets, respectively.

to concentrate excessively in localized regions, hindering the global adaptability. After applying the sensitivity-aware penalties, the parameter updates become more balanced and distributed, effectively decentralizing the adaptation burden from a few parameters to a broader set. This redistribution helps mitigate adaptation risk and promotes more stable fine-tuning.

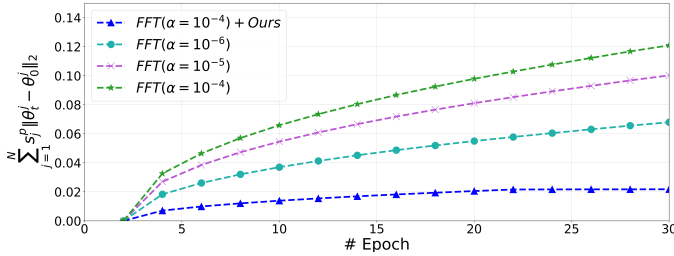


Fig. 9. Sensitivity-weighted weight distances between our regularized tuning method and the full fine-tuning (with different learning rates) on the DepthTrack.

D. Computational Efficiency

In addition to tracking accuracy, we evaluate the computational efficiency of our sensitivity-aware regularization tuning by analyzing both training and inference overhead.

Efficiency of Regularized Fine-tuning. We compare the training efficiency of our method against vanilla fine-tuning. Since prior sensitivity estimation is conducted as a one-time preprocessing step before fine-tuning, its runtime is excluded from the training time. Our method introduces parameter-wise transfer sensitivity quantification with marginal computational

TABLE XII
COMPUTATIONAL COMPLEXITY AND SPEED ANALYSIS ON THE LASHER DATASET.

Method	Base Model	Param (M)	Flops (G)	FPS	SR	PR
OSTrack [5]	OSTrack	92.1	58.1	98.4	47.2	58.5
ProTrack [41]	OSTrack	92.7	58.4	92.3	42.0	53.8
ViPT [15]	OSTrack	92.9	59.9	88.6	52.5	65.1
SDSTrack [16]	OSTrack	102.1	108.7	44.6	53.1	66.5
UnTrack [17]	OSTrack	98.7	62.6	75.6	51.3	63.7
ViPT+Ours	OSTrack	92.9	59.9	88.6	54.9	68.4
UnTrack+Ours	OSTrack	98.7	62.6	75.6	54.0	67.4
Ours	OSTrack	202.0	149.0	49.0	56.3	70.1
DropTrack [40]	DropTrack	92.1	130.6	57.6	47.7	59.2
ViPT [15]	DropTrack	92.9	131.9	48.8	52.5	65.6
SDSTrack [16]	DropTrack	102.1	244.2	26.8	55.1	69.0
UnTrack [17]	DropTrack	98.7	138.2	42.3	52.4	65.9
ViPT+Ours	DropTrack	92.9	131.9	48.8	57.1	70.5
UnTrack+Ours	DropTrack	98.7	138.2	42.3	56.3	69.4
Ours	DropTrack	202.0	335.3	29.2	58.8	73.6
SUTrack [8]	SUTrack	65.29	106.9	37.6	60.8	75.6
Ours	SUTrack	141.1	243.7	24.8	62.9	77.8

overhead, as this sensitivity is derived from the off-the-shelf gradients. While vanilla fine-tuning operates at 37.5 ms per iteration, our method runs at 39.0 ms per iteration, incurring only a modest 4.0% increase in training time.

Inference Cost and Speed. We compare the computational complexity and runtime efficiency of existing methods, focusing on models built upon OSTrack, DropTrack and SUTrack. Note that the proposed regularization techniques are applied only during training, imposing no additional computational

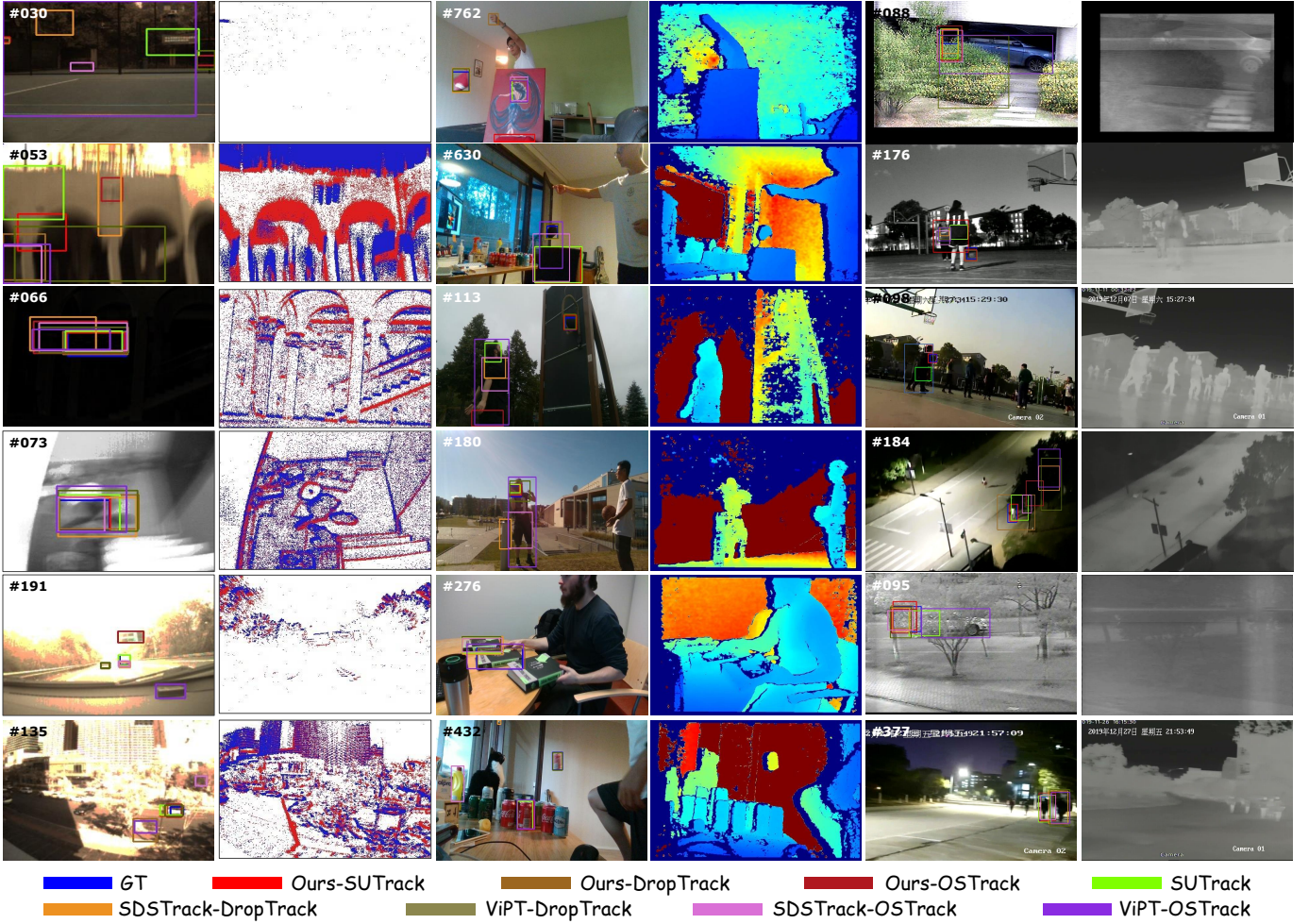


Fig. 10. Visual comparisons of the tracking performance of different methods on the (Left) RGB-Event, (Middle) RGB-Depth and (Right) RGB-Thermal datasets.

burden during testing. All experiments are conducted on the same system, which includes an Intel(R) Xeon(R) 6456C CPU, 256 GB RAM, and one NVIDIA 3090Ti GPU. As reported in Tab. XII, our method supports real-time tracking at 24.8 frames per second, while delivering top-tier performance. When integrated into ViPT, our approach (“ViPT+Ours”) yields both superior speed and performance. Under the DropTrack base model, it still operates at 48.8 frames per second, maintaining a respectable speed given its focus on accuracy.

E. Visual Comparison

Some representative visualization results are illustrated in Fig. 10. For clarity, all visual instances are explicitly labeled by the predicted bounding box. Horizontally, each instance is represented by a pair of pictures - the right image shows the main view, while the left displays the auxiliary modality. Our method demonstrates a marked improvement over state-of-the-art multi-modal methods, especially in handling complex scenarios where cross-modal integration plays a crucial role. It excels in tracking in conditions like motion blur, occlusions, and low illumination, where other methods struggle. These results demonstrate that our method improves tracking accuracy

and provides a more stable, efficient way to integrate auxiliary data.

V. CONCLUSION

This study revisits the critical misfitting issues encountered when adapting pre-trained RGB trackers to multi-modal tracking tasks. By introducing two complementary sensitivities that capture the dynamic shift in parameter importance as models transition from pre-trained to multi-modal contexts, our regularized tuning method strategically calibrates gradient updates. Extensive experiments demonstrate the effectiveness of our method, surpassing current state-of-the-art techniques across various multi-modal tracking scenarios, with notable performance improvements resulting from the incorporation of regularization. A key insight from our work is the importance of sensitivity-aware fine-tuning, which offers superior generalization and adaptability compared to traditional fine-tuning methods. Ultimately, our findings highlight the need for more nuanced cross-domain generalization strategies, as overly rigid or flexible fine-tuning can hinder pre-trained model transferability. We believe these insights will pave the way for further advancements in multi-modal transfer learning, particularly in the context of scene perception tasks.

APPENDIX

Proof of Proposition 1.

1. **Bounded FIM Error.** Each group approximation $\tilde{\mathcal{F}}(\theta_0^j)$ captures the principal tangent of $\mathcal{F}(\theta_0^j)$ with bounded error. Due to symmetry and orthogonal eigenvectors, the Frobenius norm of the error is derived from the difference in their eigenvalues:

$$\|\mathcal{F}(\theta_0^j) - \tilde{\mathcal{F}}(\theta_0^j)\|_F = \sqrt{\sum_{i=1}^{|\theta^j|} (\lambda_i^j - \gamma^j)^2},$$

Since γ^j lies between the largest and smallest eigenvalues of $\mathcal{F}(\theta_0^j)$, i.e., $\lambda_{|\theta^j|}^j < \gamma^j < \lambda_1^j$, we can deduce that:

$$\|\mathcal{F}(\theta_0^j) - \tilde{\mathcal{F}}(\theta_0^j)\|_F \leq \sqrt{\sum_{i=K+1}^{|\theta^j|} (\lambda_i^j)^2},$$

Summing over all groups, the total discarded eigenvalue mass is:

$$\|\mathcal{F}(\theta_0) - \tilde{\mathcal{F}}(\theta_0)\|_F \leq \sqrt{\sum_{j=1}^N \sum_{i=K+1}^{|\theta^j|} (\lambda_i^j)^2},$$

In particular, under the common assumption that the top- K eigenvalues in each group capture the most significant curvature, where $\text{Tr}(\mathcal{F}(\theta_0) - \tilde{\mathcal{F}}(\theta_0)) \ll \text{Tr}(\mathcal{F}(\theta_0))$, the residual eigenvalue mass is small.

2. **Bounded Generalization Gap Error.** The approximate FIM $\tilde{\mathcal{F}}(\theta_0)$ remains close to $\mathcal{F}(\theta_0)$ as a metric on parameter space. For any parameter difference $\Delta\theta \in \mathbb{R}^{|\theta|}$, let $\varepsilon_{\text{gen}}(\mathcal{F}(\theta_0)) = \frac{1}{2}\Delta\theta^T \mathcal{F}(\theta_0) \Delta\theta$ denote the generalization gap induced by the true FIM. Likewise $\varepsilon_{\text{gen}}(\tilde{\mathcal{F}}(\theta_0)) = \frac{1}{2}\Delta\theta^T \tilde{\mathcal{F}}(\theta_0) \Delta\theta$ is the approximated generalization gap. Then the discrepancy between these distances is bounded in terms of the residual generalization gap error. In particular, one has following formula by definition of the spectral norm:

$$|\varepsilon_{\text{gen}}(\mathcal{F}(\theta_0)) - \varepsilon_{\text{gen}}(\tilde{\mathcal{F}}(\theta_0))| \leq \frac{1}{2} \|\mathcal{F}(\theta_0) - \tilde{\mathcal{F}}(\theta_0)\|_2 \|\Delta\theta\|^2,$$

Since $\mathcal{F}(\theta_0) - \tilde{\mathcal{F}}(\theta_0)$ is group-diagonal (with each block $\mathcal{F}(\theta_0^j) - \tilde{\mathcal{F}}(\theta_0^j)$) and symmetric, its spectral norm is:

$$\|\mathcal{F}(\theta_0) - \tilde{\mathcal{F}}(\theta_0)\|_2 = \max_{1 \leq j \leq N} \|\mathcal{F}(\theta_0^j) - \tilde{\mathcal{F}}(\theta_0^j)\|_2,$$

Using the bound above, we obtain

$$|\varepsilon_{\text{gen}}(\mathcal{F}(\theta_0)) - \varepsilon_{\text{gen}}(\tilde{\mathcal{F}}(\theta_0))| \leq \frac{1}{2} \|\Delta\theta\|^2 \left(\max_{1 \leq j \leq N} \lambda_1^j \right),$$

Specifically, due to the general principle that the spectral norm of a symmetric matrix is always smaller than its Frobenius norm, we can also derive:

$$|\varepsilon_{\text{gen}}(\mathcal{F}(\theta_0)) - \varepsilon_{\text{gen}}(\tilde{\mathcal{F}}(\theta_0))| \leq \frac{1}{2} \|\Delta\theta\|^2 \sqrt{\sum_{i=K+1}^{|\theta^j|} (\lambda_i^j)^2},$$

In practice, by retaining the top- K eigenvalues in each FIM block (which capture the majority of the FIM energy)

and replacing the remaining eigenvalues with an isotropic average, one obtains a low-rank Fisher matrix approximation that preserves the important Riemannian geometry of the parameter space while bounding the distortion in any distance or generalization metric by the residual eigenvalue mass.

REFERENCES

- [1] L. Hong, S. Yan, R. Zhang, W. Li, X. Zhou, P. Guo, K. Jiang, Y. Chen, J. Li, Z. Chen *et al.*, “Onetracker: Unifying visual object tracking with foundation models and efficient tuning,” in *Proceedings of the IEEE/CVF Conference on Computer Vision and Pattern Recognition*, 2024, pp. 19079–19091.
- [2] F. Xie, Z. Wang, and C. Ma, “Diffusiontrack: Point set diffusion model for visual object tracking,” in *Proceedings of the IEEE/CVF Conference on Computer Vision and Pattern Recognition*, 2024, pp. 19113–19124.
- [3] G. Zheng, S. Lin, H. Zuo, C. Fu, and J. Pan, “Nettrack: Tracking highly dynamic objects with a net,” in *Proceedings of the IEEE/CVF Conference on Computer Vision and Pattern Recognition*, 2024, pp. 19145–19155.
- [4] W. Cai, Q. Liu, and Y. Wang, “Hiptrack: Visual tracking with historical prompts,” in *Proceedings of the IEEE/CVF Conference on Computer Vision and Pattern Recognition*, 2024, pp. 19258–19267.
- [5] B. Ye, H. Chang, B. Ma, S. Shan, and X. Chen, “Joint feature learning and relation modeling for tracking: A one-stream framework,” in *European Conference on Computer Vision*. Springer, 2022, pp. 341–357.
- [6] L. Lin, H. Fan, Z. Zhang, Y. Xu, and H. Ling, “Swintrack: A simple and strong baseline for transformer tracking,” *Advances in Neural Information Processing Systems*, vol. 35, pp. 16743–16754, 2022.
- [7] X. Chen, H. Peng, D. Wang, H. Lu, and H. Hu, “Seqtrack: Sequence to sequence learning for visual object tracking,” in *Proceedings of the IEEE/CVF conference on computer vision and pattern recognition*, 2023, pp. 14572–14581.
- [8] X. Chen, B. Kang, W. Geng, J. Zhu, Y. Liu, D. Wang, and H. Lu, “Sutrack: Towards simple and unified single object tracking,” in *Proceedings of the AAAI Conference on Artificial Intelligence*, vol. 39, no. 2, 2025, pp. 2239–2247.
- [9] X. Wang, J. Li, L. Zhu, Z. Zhang, Z. Chen, X. Li, Y. Wang, Y. Tian, and F. Wu, “Visevent: Reliable object tracking via collaboration of frame and event flows,” *IEEE Transactions on Cybernetics*, 2023.
- [10] Z. Zhu, J. Hou, and D. O. Wu, “Cross-modal orthogonal high-rank augmentation for rgb-event transformer-trackers,” in *Proceedings of the IEEE/CVF International Conference on Computer Vision*, 2023, pp. 22045–22055.
- [11] C. Sun, J. Zhang, Y. Wang, H. Ge, Q. Xia, B. Yin, and X. Yang, “Exploring historical information for rgb event tracking with mamba,” in *Proceedings of the Computer Vision and Pattern Recognition Conference (CVPR)*, June 2025, pp. 6500–6509.
- [12] E. J. Hu, Y. Shen, P. Wallis, Z. Allen-Zhu, Y. Li, S. Wang, L. Wang, and W. Chen, “Lora: Low-rank adaptation of large language models,” *arXiv preprint arXiv:2106.09685*, 2021.
- [13] M. Jia, L. Tang, B.-C. Chen, C. Cardie, S. Belongie, B. Hariharan, and S.-N. Lim, “Visual prompt tuning,” in *European Conference on Computer Vision*. Springer, 2022, pp. 709–727.
- [14] S. Chen, C. Ge, Z. Tong, J. Wang, Y. Song, J. Wang, and P. Luo, “Adaptformer: Adapting vision transformers for scalable visual recognition,” *Advances in Neural Information Processing Systems*, vol. 35, pp. 16664–16678, 2022.
- [15] J. Zhu, S. Lai, X. Chen, D. Wang, and H. Lu, “Visual prompt multi-modal tracking,” in *Proceedings of the IEEE/CVF conference on computer vision and pattern recognition*, 2023, pp. 9516–9526.
- [16] X. Hou, J. Xing, Y. Qian, Y. Guo, S. Xin, J. Chen, K. Tang, M. Wang, Z. Jiang, L. Liu *et al.*, “Sdstrack: Self-distillation symmetric adapter learning for multi-modal visual object tracking,” in *Proceedings of the IEEE/CVF Conference on Computer Vision and Pattern Recognition*, 2024, pp. 26551–26561.
- [17] Z. Wu, J. Zheng, X. Ren, F.-A. Vasluianu, C. Ma, D. P. Paudel, L. Van Gool, and R. Timofte, “Single-model and any-modality for video object tracking,” in *Proceedings of the IEEE/CVF Conference on Computer Vision and Pattern Recognition*, 2024, pp. 19156–19166.
- [18] X. Wei, Y. Bai, Y. Zheng, D. Shi, and Y. Gong, “Autoregressive visual tracking,” in *Proceedings of the IEEE/CVF conference on computer vision and pattern recognition*, 2023, pp. 9697–9706.

- [19] Y. Bai, Z. Zhao, Y. Gong, and X. Wei, "Artrackv2: Prompting autoregressive tracker where to look and how to describe," in *Proceedings of the IEEE/CVF conference on computer vision and pattern recognition*, 2024, pp. 19048–19057.
- [20] L. Lin, H. Fan, Z. Zhang, Y. Wang, Y. Xu, and H. Ling, "Tracking meets lora: Faster training, larger model, stronger performance," in *European Conference on Computer Vision*. Springer, 2024, pp. 300–318.
- [21] Y. Zheng, B. Zhong, Q. Liang, Z. Mo, S. Zhang, and X. Li, "Odtrack: Online dense temporal token learning for visual tracking," in *Proceedings of the AAAI conference on artificial intelligence*, vol. 38, no. 7, 2024, pp. 7588–7596.
- [22] Y. Zhang, Q. Zhang, Z. Zhu, J. Hou, and Y. Yuan, "Glenet: Boosting 3d object detectors with generative label uncertainty estimation," *International Journal of Computer Vision*, vol. 131, no. 12, pp. 3332–3352, 2023.
- [23] Z. Zhu, J. Hou, and X. Lyu, "Learning graph-embedded key-event back-tracing for object tracking in event clouds," *Advances in Neural Information Processing Systems*, vol. 35, pp. 7462–7476, 2022.
- [24] Z. Chen, J. Wu, W. Dong, L. Li, and G. Shi, "Crossei: Boosting motion-oriented object tracking with an event camera," *IEEE Transactions on Image Processing*, 2024.
- [25] X. Wang, S. Wang, C. Tang, L. Zhu, B. Jiang, Y. Tian, and J. Tang, "Event stream-based visual object tracking: A high-resolution benchmark dataset and a novel baseline," in *Proceedings of the IEEE/CVF Conference on Computer Vision and Pattern Recognition (CVPR)*, June 2024, pp. 19248–19257.
- [26] T. Zhang, K. Debatista, Q. Zhang, J. Han *et al.*, "Revisiting motion information for rgb-event tracking with mot philosophy," *Advances in Neural Information Processing Systems*, vol. 37, pp. 89346–89372, 2024.
- [27] S. Wang, J. Huang, Q. Ma, J. Gao, C. Xu, X. Wang, L. Chen, and B. Jiang, "Mamba-fetrack v2: Revisiting state space model for frame-event based visual object tracking," *arXiv preprint arXiv:2506.23783*, 2025.
- [28] S. Wang, X. Wang, L. Jin, B. Jiang, L. Zhu, L. Chen, Y. Tian, and B. Luo, "Towards low-latency event stream-based visual object tracking: A slow-fast approach," *arXiv preprint arXiv:2505.12903*, 2025.
- [29] A. Lukežić, U. Kart, J. Kapyla, A. Durmush, J.-K. Kamarainen, J. Matas, and M. Kristan, "Cdtb: A color and depth visual object tracking dataset and benchmark," in *Proceedings of the IEEE/CVF International Conference on Computer Vision*, 2019, pp. 10013–10022.
- [30] Y. Qian, S. Yan, A. Lukežić, M. Kristan, J.-K. Kamarainen, and J. Matas, "Dal: A deep depth-aware long-term tracker," in *2020 25th International conference on pattern recognition (ICPR)*. IEEE, 2021, pp. 7825–7832.
- [31] S. Yan, J. Yang, J. Käpylä, F. Zheng, A. Leonardis, and J.-K. Kamarainen, "Depthtrack: Unveiling the power of rgbd tracking," in *Proceedings of the IEEE/CVF International Conference on Computer Vision*, 2021, pp. 10725–10733.
- [32] Z. Liu, X. Wang, C. Wang, W. Liu, and X. Bai, "Sparsetrack: Multi-object tracking by performing scene decomposition based on pseudo-depth," *IEEE Transactions on Circuits and Systems for Video Technology*, vol. 35, no. 5, pp. 4870–4882, 2025.
- [33] P. Zhang, J. Zhao, C. Bo, D. Wang, H. Lu, and X. Yang, "Jointly modeling motion and appearance cues for robust rgb-t tracking," *IEEE Transactions on Image Processing*, vol. 30, pp. 3335–3347, 2021.
- [34] T. Hui, Z. Xun, F. Peng, J. Huang, X. Wei, X. Wei, J. Dai, J. Han, and S. Liu, "Bridging search region interaction with template for rgb-t tracking," in *Proceedings of the IEEE/CVF Conference on Computer Vision and Pattern Recognition*, 2023, pp. 13630–13639.
- [35] S. Li, R. Yao, Y. Zhou, H. Zhu, K. Sun, B. Liu, Z. Shao, and J. Zhao, "Modality-guided dynamic graph fusion and temporal diffusion for self-supervised rgb-t tracking," 2025. [Online]. Available: <https://arxiv.org/abs/2505.03507>
- [36] X. Xiang, Q. Yan, H. Zhang, and J. Ma, "Acattack: Adaptive cross attacking rgb-t tracker via multi-modal response decoupling," in *Proceedings of the Computer Vision and Pattern Recognition Conference (CVPR)*, June 2025, pp. 22099–22108.
- [37] C. Tang, X. Wang, J. Huang, B. Jiang, L. Zhu, J. Zhang, Y. Wang, and Y. Tian, "Revisiting color-event based tracking: A unified network, dataset, and metric," *arXiv preprint arXiv:2211.11010*, 2022.
- [38] J. Zhang, B. Dong, Y. Fu, Y. Wang, X. Wei, B. Yin, and X. Yang, "A universal event-based plug-in module for visual object tracking in degraded conditions," *International Journal of Computer Vision*, vol. 132, no. 5, pp. 1857–1879, 2024.
- [39] Y. Zhang, Q. Zhang, J. Hou, Y. Yuan, and G. Xing, "Unleash the potential of image branch for cross-modal 3d object detection," *Advances in Neural Information Processing Systems*, vol. 36, pp. 51562–51583, 2023.
- [40] Q. Wu, T. Yang, Z. Liu, B. Wu, Y. Shan, and A. B. Chan, "Dropmae: Masked autoencoders with spatial-attention dropout for tracking tasks," in *Proceedings of the IEEE/CVF Conference on Computer Vision and Pattern Recognition*, 2023, pp. 14561–14571.
- [41] J. Yang, Z. Li, F. Zheng, A. Leonardis, and J. Song, "Prompting for multi-modal tracking," in *Proceedings of the 30th ACM international conference on multimedia*, 2022, pp. 3492–3500.
- [42] B. Cao, J. Guo, P. Zhu, and Q. Hu, "Bi-directional adapter for multi-modal tracking," in *Proceedings of the AAAI Conference on Artificial Intelligence*, vol. 38, no. 2, 2024, pp. 927–935.
- [43] M. Mermillod, A. Bugaiska, and P. Bonin, "The stability-plasticity dilemma: Investigating the continuum from catastrophic forgetting to age-limited learning effects," p. 504, 2013.
- [44] S.-i. Amari, R. Karakida, and M. Oizumi, "Fisher information and natural gradient learning in random deep networks," in *The 22nd International Conference on Artificial Intelligence and Statistics*. PMLR, 2019, pp. 694–702.
- [45] Y. Liu, S. Mai, X. Chen, C.-J. Hsieh, and Y. You, "Towards efficient and scalable sharpness-aware minimization," in *Proceedings of the IEEE/CVF Conference on Computer Vision and Pattern Recognition*, 2022, pp. 12360–12370.
- [46] X. Wu, W. Yu, C. Zhang, and P. Woodland, "An improved empirical fisher approximation for natural gradient descent," *Advances in Neural Information Processing Systems*, vol. 37, pp. 134151–134194, 2024.
- [47] B. Ghorbani, S. Krishnan, and Y. Xiao, "An investigation into neural net optimization via hessian eigenvalue density," in *International Conference on Machine Learning*. PMLR, 2019, pp. 2232–2241.
- [48] A. Rame, C. Dancette, and M. Cord, "Fislr: Invariant gradient variances for out-of-distribution generalization," in *International Conference on Machine Learning*. PMLR, 2022, pp. 18347–18377.
- [49] R.-C. Li, "Rayleigh quotient based optimization methods for eigenvalue problems," *Matrix Functions and Matrix Equations*, vol. 19, pp. 76–108, 2015.
- [50] R. J. LeVeque, "Finite difference methods for differential equations," *Draft version for use in AMath*, vol. 585, no. 6, p. 112, 1998.
- [51] N. Hurley and S. Rickard, "Comparing measures of sparsity," *IEEE Transactions on Information Theory*, vol. 55, no. 10, pp. 4723–4741, 2009.
- [52] Y. Nesterov, *Introductory lectures on convex optimization: A basic course*. Springer Science & Business Media, 2013, vol. 87.
- [53] J. Zhang, X. Yang, Y. Fu, X. Wei, B. Yin, and B. Dong, "Object tracking by jointly exploiting frame and event domain," in *Proceedings of the IEEE/CVF International Conference on Computer Vision*, 2021, pp. 13043–13052.
- [54] M. Kristan, A. Leonardis, J. Matas, M. Felsberg, R. Pflugfelder, J.-K. Kamarainen, H. J. Chang, M. Danelljan, L. Č. Zajc, A. Lukežić *et al.*, "The tenth visual object tracking vot2022 challenge results," in *European Conference on Computer Vision*. Springer, 2022, pp. 431–460.
- [55] C. Li, L. Liu, A. Lu, Q. Ji, and J. Tang, "Challenge-aware rgbt tracking," in *European conference on computer vision*. Springer, 2020, pp. 222–237.
- [56] C. Li, X. Liang, Y. Lu, N. Zhao, and J. Tang, "Rgb-t object tracking: Benchmark and baseline," *Pattern Recognition*, vol. 96, p. 106977, 2019.
- [57] A. Dosovitskiy, L. Beyer, A. Kolesnikov, D. Weissenborn, X. Zhai, T. Unterthiner, M. Dehghani, M. Minderer, G. Heigold, S. Gelly *et al.*, "An image is worth 16x16 words: Transformers for image recognition at scale," *arXiv preprint arXiv:2010.11929*, 2020.
- [58] X. Zhang, Y. Tian, L. Xie, W. Huang, Q. Dai, Q. Ye, and Q. Tian, "Hivit: A simpler and more efficient design of hierarchical vision transformer," in *The eleventh international conference on learning representations*, 2023.
- [59] G. Bhat, M. Danelljan, L. V. Gool, and R. Timofte, "Learning discriminative model prediction for tracking," in *Proceedings of the IEEE/CVF international conference on computer vision*, 2019, pp. 6182–6191.
- [60] B. Yan, H. Peng, J. Fu, D. Wang, and H. Lu, "Learning spatio-temporal transformer for visual tracking," in *Proceedings of the IEEE/CVF international conference on computer vision*, 2021, pp. 10448–10457.
- [61] J. Zhang, Y. Wang, W. Liu, M. Li, J. Bai, B. Yin, and X. Yang, "Frame-event alignment and fusion network for high frame rate tracking," in *Proceedings of the IEEE/CVF Conference on Computer Vision and Pattern Recognition*, 2023, pp. 9781–9790.
- [62] X.-F. Zhu, T. Xu, Z. Tang, Z. Wu, H. Liu, X. Yang, X.-J. Wu, and J. Kittler, "Rgbdlk: A large-scale dataset and benchmark for rgb-d object tracking," in *Proceedings of the AAAI Conference on Artificial Intelligence*, vol. 37, no. 3, 2023, pp. 3870–3878.

- [63] Y. Xiao, M. Yang, C. Li, L. Liu, and J. Tang, "Attribute-based progressive fusion network for rgbt tracking," in *Proceedings of the AAAI Conference on Artificial Intelligence*, vol. 36, no. 3, 2022, pp. 2831–2838.
- [64] H. Rebecq, T. Horstschaefer, and D. Scaramuzza, "Real-time visual-inertial odometry for event cameras using keyframe-based nonlinear optimization," in *British Machine Vision Conference*, 2017.
- [65] A. I. Maqueda, A. Loquercio, G. Gallego, N. García, and D. Scaramuzza, "Event-based vision meets deep learning on steering prediction for self-driving cars," in *Proceedings of the IEEE conference on computer vision and pattern recognition*, 2018, pp. 5419–5427.
- [66] A. Sironi, M. Brambilla, N. Bourdis, X. Lagorce, and R. Benosman, "Hats: Histograms of averaged time surfaces for robust event-based object classification," in *Proceedings of the IEEE conference on computer vision and pattern recognition*, 2018, pp. 1731–1740.
- [67] H. Chen, D. Suter, Q. Wu, and H. Wang, "End-to-end learning of object motion estimation from retinal events for event-based object tracking," in *Proceedings of the AAAI Conference on Artificial Intelligence*, vol. 34, no. 07, 2020, pp. 10534–10541.
- [68] A. Z. Zhu, L. Yuan, K. Chaney, and K. Daniilidis, "Unsupervised event-based learning of optical flow, depth, and egomotion," in *Proceedings of the IEEE/CVF Conference on Computer Vision and Pattern Recognition*, 2019, pp. 989–997.



Junhui Hou (Senior Member, IEEE) is an Associate Professor with the Department of Computer Science, City University of Hong Kong. He holds a B.Eng. degree in information engineering (Talented Students Program) from the South China University of Technology, Guangzhou, China (2009), an M.Eng. degree in signal and information processing from Northwestern Polytechnical University, Xi'an, China (2012), and a Ph.D. degree from the School of Electrical and Electronic Engineering, Nanyang Technological University, Singapore (2016). His research interests are multi-dimensional visual computing.

Dr. Hou received the Early Career Award (3/381) from the Hong Kong Research Grants Council in 2018 and the NSFC Excellent Young Scientists Fund in 2024. He has served or is serving as an Associate Editor for *IEEE Transactions on Visualization and Computer Graphics*, *IEEE Transactions on Image Processing*, *IEEE Transactions on Multimedia*, and *IEEE Transactions on Circuits and Systems for Video Technology*.



Zhiwen Chen received the B.E. and M.E. degrees in Measurement and control technology, both from Xidian University, in 2019 and 2021, respectively. He has also received a Ph.D. degree in Computer Science from the Xidian University in 2025. His research interests include event-based vision and scene perception.



Zhiyu Zhu received the B.E. and M.E. degrees in Mechatronic Engineering, both from Harbin Institute of Technology, in 2017 and 2019, respectively. He has also received a Ph.D. degree in Computer Science from the City University of Hong Kong in 2023, where he currently holds a postdoctoral position. His research interests include generative models and computer vision.



Yifan Zhang received the B.E. degree from the Huazhong University of Science and Technology (HUST), the M.E. degree from Shanghai Jiao Tong University (SJTU), and the Ph.D. degree from the Department of Computer Science, City University of Hong Kong. Since 2025, he has been a lecturer at Shanghai University. His research interests include deep learning and 3D scene understanding.



Jinjian Wu (Senior Member, IEEE) received the B.Sc. and Ph.D. degrees from Xidian University, Xi'an, China, in 2008 and 2013, respectively. From 2011 to 2013, he was a Research Assistant with Nanyang Technological University, Singapore, where he was a Post-Doctoral Research Fellow from 2013 to 2014. From 2015 to 2019, he was an Associate Professor with Xidian University, where he has been a Professor since 2019. His research interests include visual perceptual modeling, biomimetic imaging, quality assessment, and object detection.

He received the Best Student Paper Award with ISCAS, in 2013. He has served as an associate editor for the Journal of Circuits, Systems, and Signal Processing, the special section chair for IEEE Visual Communications and Image Processing, in 2017, and the section chair/an organizer/a TPC member for ICME from 2014 to 2015, PCM from 2015 to 2016, ICIP in 2015, VCIP in 2018, and AAAI in 2019.